Summer 2020

Investigation of Oxidized Carbon Supported AU Catalysts Synthesized via Strong Electrostatic Adsorption of $AU(en)_2Cl_3$ for the Hydrochlorination of Acetylene to Vinyl Chloride Monomer

Sean Reginald Noble

Investigation of Oxidized carbon supported Au catalysts synthesized via Strong Electrostatic Adsorption of $Au(en)_2Cl_3$ for the Hydrochlorination of Acetylene to Vinyl Chloride Monomer

By

Sean Reginald Noble

Bachelor of Science
University of Missouri, 2015

Submitted in Partial Fulfillment of the Requirements

For the Degree of Doctor of Philosophy in

Chemical Engineering

College of Engineering and Computing

University of South Carolina

2020

Accepted by:

John R. Reglabuto, Major Professor

John R. Monnier, Major Professor

Christopher T. Williams, Committee Member

Aaron K. Vannucci, Committee Member

Melissa Moss, Committee Member

Cheryl L. Addy, Vice Provost and Dean of Graduate Studies

Acknowledgements

I would first like to give honor to God who is the head of my life for the strength to persevere and for grace in my growth. I would like to thank all of the people who have helped me and poured into me at the university of South Carolina like Dr. Andrew Wong, Dr. Jayson Keels, Dr. Sonia Eskandari, Gregory Tate, Ben Egelske, and Mozdeh Parizad. I want to thank my advisors Dr. John Regalbuto for his energy and patience throughout this process and Dr. John Monnier for his hands on guidance and tough love allowing me to develop a depth of knowledge over the field of catalysis. Thank you Dr. Aaron Vannucci for teaching me to work with purpose when researching and not just the acquisition of data. Thank you to everyone on my PhD committee for your knowledge and probing questions that helped me to focus and further my research, Dr. Chris Williams and Dr. John Weidner.

I want to thank my family for cheering me on and having faith in me. Thank you to my Father and Mother, Sean and Katrice Noble for raising me to be a thinker and have ambitious goals. Thank you to my mother Rosalyn Wilson for showing me the principles of hard work and determination. Thank you to my Grandparents Willia Clayborn, Albert Noble, Dorothy Wilson, and Donald Wilson for all of the love, support, provision, and prayer. Thank you to my many younger siblings T'Keyah, Keith, Elijah, Eryckah, Devin, Jordan, Jaden, Solomon, and Mckenzie for being my inspiration to succeed knowing that you are looking up to me. Thank you to my Young Life family and my church family at Forward City Church for allowing me to be in community and becoming my family.

Without my support network I would not have been able to stable and accomplish this task and I am forever grateful for you.

Abstract

Over 20 million tons of vinyl chloride monomer (VCM) is produced every year using acetylene hydrochlorination using a supported mercuric chloride catalyst. During this process mercury is reduced and sublimes into the environment harming all living animals and humans, so carbon-supported Au catalysts have been developed in attempts to replace it. Various techniques have been used to make these catalysts including several variations of dry impregnation. In this study we investigate the ability of Strong Electrostatic Adsorption (SEA) of $Au(en)_2Cl_3$ onto various supports to demonstrate the ability to rationally and consistently synthesize gold catalysts with ultra-small particle sizes. The supports include carbon, silica, titania, zirconia, ceria, and alumina.

SEA of $Au(en)_2Cl_3$ is employed with oxidized Norit Rox carbon as the support for the acetylene hydrochlorination reaction and results in greater activity and stability when compared to other carbon supports. The hydroxyl group content on Norit Rox which results from oxidation of the support facilitates high uptake of the $Au(en)_2Cl_3$ during SEA. XPS studies revealed that Norit Rox has 5 times the surface area of sp^3 hybridized carbon, which are indictive of defect sites in the predominant sp^2 hybridized carbon substrate, when compared to Timrex. It is hypothesized that these defects are stable binding sites for the active $AuCl_3$ site. During HCl pretreatment gold nanoparticles on most carbon supports sinter, but because Norit Rox has an abundance of stable binding sites for the active $AuCl_3$ species, the HCl pretreatment results in a redispersion of

Au, including nanoparticles up to 4 nm in size, into atomically dispersed $AuCl_3$. Norit Rox also can adsorb up to 3 times more Cl onto its surface during pretreatment, permitting the addition of Cl to Au during the reaction process. There is a direct correlation between the sp^3 surface area and the acetylene conversion, and Cl adsorption during pretreatment and reaction. When compared to the leading catalysts made with the traditional $HAuCl_4$ and aqua regia method, catalysts synthesized by SEA using $Au(en)_2Cl_3$ precursor are more active and stable.

Table of Contents

List of Tables

List of Figures

Chapter 1

A Review of Catalyst Synthesis for Acetylene Hydrochlorination Reaction

1.1 Introduction

Supported metal catalysts have long been used in numerous industrial processes for decades but the potential for gold to be used in catalytic processes has developed more recently. In the 1980's two very important discoveries were made that gave momentum in the study of gold catalysts. In 1987 Haruta showed that gold nanoparticles supported on transition metal oxides were able to be used in the low temperature oxidation of CO.[1] Additionally in 1985 Hutchings predicted and soon after confirmed that gold was the most active metal for acetylene hydrochlorination catalyzed by a carbon supported metal catalyst.[2,3] Later in 1996 gold on FeO and TiO_2 were found to be active for low temperature water gas shift.[4] Prior to the 1980s gold was largely considered unreactive in spite of being reported for the selective oxidation of hydrocarbons and reduction of NO and olefins.[5] A review of the early history of gold catalysis before 1980 shows that there were hundreds of articles before 1980 that show gold being used catalytically for processes such as hydrogenation, dehydrogenation, reactions involving halogen atoms, oxidation, oxidative dehydrogenation, and even as fuel cell electrodes.[6] Another review paper summarizes studies of gold being used for chemoselective hydrogenation of unsaturated aldehydes and selective partial hydrogenation of alkyne, alkadiene, and alkene hydrocarbon streams.[7]

In the last few decades much research has been done in the production of vinyl chloride monomer (VCM) using acetylene hydrochlorination over a carbon supported gold catalyst. VCM is the one of largest produced commodity chemicals by volume with a production of over 50 million tons a year and is the monomer used to make polyvinyl chloride (PVC) which is one of the top three plastic polymers produced per year by volume. PVC has many uses including construction materials, medical devices, clothing and packaging. The clear majority of VCM is used in PVC production with its alternative use being in the manufacture of chlorinated solvents. Due to this relationship the growth projections of both are deeply intertwined.

VCM is produced through oxychlorination of ethylene or acetylene hydrochlorination. The most common route, oxychlorination of ethylene, is a balance process and is utilized in the United States due to the availability of oil. It is a combination of chlorination and oxychlorination reactions using ethylene, which is an oil derived starting material. The reaction equations as follows:

(1.1) $C_2H_4 + Cl_2 \rightarrow CH_2ClCH_2Cl$

(1.2) $C_2H_4 + 2HCl + \frac{1}{2} O_2 \rightarrow CH_2ClCH_2Cl + H_2O$

(1.3) $CH_2ClCH_2Cl \rightarrow CH_2CHCl + HCl$

The first step is the direct chlorination step of ethylene to 1,2-Dichloroethane (DCE) (Equation 1.1). Step 2 is the oxichlorination step that produces DCE and water (Equation 1.2). The product streams of the first two steps are then purified before step 3 which is thermal cracking to form VCM and HCl (Equation 1.3). The downside of this process is that it is a multi-step process which means that it is more expensive. Additionally,

the final product stream contains HCl and VCM so there needs to be a purification step and a recycle stream. Having a recycle stream is a difficult and possibly dangerous process.

Acetylene hydrochlorination is a much simpler route to produce VCM because it only requires one step. Acetylene is a coal derived feedstock therefore this process is utilized mostly in China due to its abundance of coal. The acetylene hydrochlorination process yields a highly pure stream of VCM and requires little further treatment and no thermal cracking compared to ethylene oxychlorination. 20 million of the 50 million tons of VCM produced is made through acetylene hydrochlorination.

(1.4) $C_2H_2 + HCl \rightarrow CH_2CHCl$

The acetylene hydrochlorination process has several drawbacks. The traditional catalysts for acetylene hydrochlorination is a mercuric chloride ($HgCl_3$) catalyst on a carbon support. Under reaction conditions the Hg is reduced and sublimes into the environment harming all living animals and humans. Due to environmental concerns and a resolution made by the United Nations, the Minatama Convention, the use of Hg for this process is being phased out and the search for an alternative catalyst has ensued for the last few decades. Carbon-supported Au catalysts have been developed in attempts to replace the traditional mercuric chloride catalyst.

1.2 Discovery of an alternative catalyst for acetylene hydrochlorination

Au supported on carbon was first identified to be the best alternative to the mercuric chloride catalyst by Hutchings using a 2 electrode standard potential as the most suitable parameter for the correlation of catalytic activity.[8] This data can be represented by a single function and can be properly used to predict catalytic activity. Later work verified that Au

on carbon is in fact highly active for this reaction system.[9] Recent work by Hutchings has discovered that the active site for the hydrochlorination reaction is an atomically dispersed Au^{+} or Au^{3+} site.[10] This was found utilizing X-Ray photo spectroscopy (XPS) ex situ experiments in combination with HAADF-STEM.

The use of XPS allows for the investigation of the oxidation state of the Au before, during, or after being in reaction, or pretreatment conditions. Au nanoparticles are known to sinter rapidly under pretreatment with HCl and under reaction conditions if they are supported on carbon regardless of how small nanoparticles are. This in turn causes deactivation of the catalyst due to the loss of available active sites. Many researchers have sought to fix the issue of sintering by making bimetallic catalysts and have met with marginal success. Any catalyst that increases the stability of Au must have the ability to maintain the oxidation state of atomically dispersed Au to Au^{+} or Au^{3+}.[11]

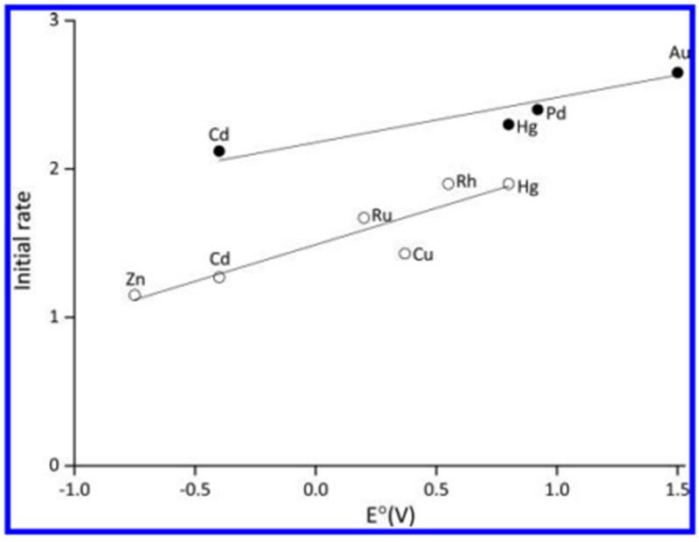

Figure 1.1: Correlation of the initial activity with the standard electrode potential for the reaction[8]

In the recent work by Hutchings an atomically dispersed Au on a carbon supported catalyst was synthesized and verified that single atoms were the catalytically active site.[12] Because the Au is atomically dispersed on Norit ROX carbon it could maintain an oxidized state under reaction conditions and resist sintering more than any other catalyst. Hutchings also found that anchoring the atomically dispersed Au is the key to making an active and stable catalyst. Au readily bonds to sites containing elements like nitrogen and sulfur strongly enough to be stable even under the harsh reaction conditions. Binding Au to these sites results in high activity even at low weight loadings approaching 0.1%.[12]

1.3 Catalyst Preparation

Dry Impregnation

Gold on carbon catalysts for acetylene hydrochlorination have been synthesized using several preparation methods. The most common and simplest method of preparation is dry impregnation (DI) or incipient wetness impregnation. This method is also called the pore filling method because the amount of solvent, typically water, is just the amount needed to fill the pores of the support. This allows for the ease of no filtration and precise metal loading. The liquid solvent diffuses throughout the macro and micro pores of the support evenly dispersing the metal salt on the surface of the support and after drying the metal species remains on the support.[13] DI does not always result in high dispersion, small particle sizes, nor strongly bonded metal because pH is not often controlled to ensure strong precursor support interaction.

Several variations of DI have been utilized in attempts to eliminate the disadvantages of DI catalysts for this reaction. The most commonly used method is DI with a concentrated aqua regia solvent.[14] Gold is known to dissolve in aqua regia so the solvent

is able to completely dissolve the $HAuCl_4$ salt and allow for deposition of small gold particles and even some atomic dispersion. The use of aqua regia is not ideal because it is highly corrosive, especially in large quantities. There have also been catalysts made using DI with aqua regia while exchanging one ligand with another. A separate ligand, like thiosulfate, is put into the solvent with the $HAuCl_4$ and is subsequently exchanged with the Cl ligands and attached to the gold upon impregnation of the support.[11] This results in atomically dispersed Au with specific ligands attached to them that result in different activities in the acetylene hydrochlorination reaction. Dry impregnation with multiple metal salts, co-DI, has been used to make bimetallic and even trimetallic gold catalysts. This method is the same as traditional DI except more than one metal salt is added to the solvent.[15–18] The reason for this method is because some secondary metals like copper, cesium, or strontium are thought to be able to stabilize gold nanoparticles and increase activity.

More recently there have been studies done where gold on carbon catalysts have been made with DI utilizing ionic liquids, such as 1-propyl-3- methylimidazolium. These catalysts are prepared by first dissolving the $HAuCl_4$ precursor in an ionic liquid, stirred at room temperature to ensure homogenization. The mixture is then combined with a minimal amount of deionized water and then added to the carbon support similar to DI.[19–21] This results in a supported ionic liquid phase on the carbon support as shown in Figure 1.2.

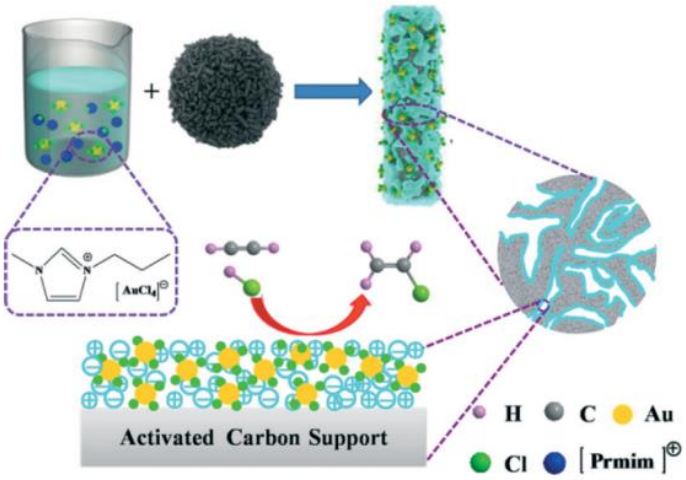

Figure 1.2: Schematic view of a supported ionic liquid phase (SILP) catalyst system[20]

Strong Electrostatic Adsorption

An effective method to strongly adsorb ultra-small gold nanoparticles and even atomically dispersed gold onto carbon is strong electrostatic adsorption (SEA). SEA is the cornerstone method of catalyst synthesis for the Regalbuto research group. [22–25] This method accounts for the charge of support surface in the adsorbing of solution as a function of pH of the solution. The control of surface pH and its ability to change the charge on the surface of a support are what sets SEA apart from the typical impregnation method. Cationic or anionic metal precursors are able adsorb onto the surface because of electrostatic interactions between the precursor and the support. The basis of SEA dates back to work done by Brunelle and Schwarz who theorized that the adsorption of noble metal complexes was columbic in nature.[26–29] The degree of protonation or deprotonation of the surface hydroxyl groups as a function of adsorbate solution pH determines if there is a driving force for either cationic or anionic precursor to adsorb onto the surface. The pH at which the net charge on the support becomes zero is called the point of zero charge or PZC.[30] This is depicted in figure 1.3.

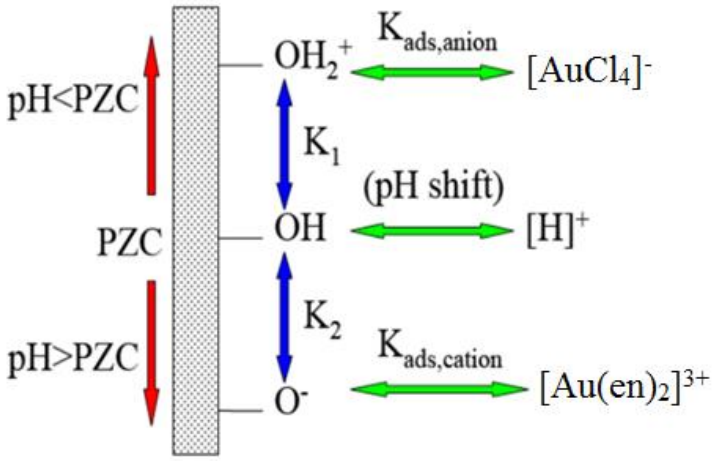

Figure 1.3: Mechanism of electrostatic adsorption for the case of Au over a charged support surface

The process through which ions adsorb onto a support surface during SEA is that individual positively or negatively charged ions bind to protonated of deprotonated hydroxyl groups. After drying in air or under vacuum at room temperature ultra-small particles may form and are covered in one or two hydration sheaths.[31,32] The catalysts are then reduced in hydrogen where hydration sheaths are removed and the metal in reduced. In some instances, like with $Au(en)_2Cl_3$ on carbons such as Norit ROX, the adsorbed gold species stays dispersed atomically and does not form nanoparticles before reduction. This means that individual $Au(en)_2^{3+}$ ions are strongly adsorbed to deprotonated hydroxyl groups on the surface of the support. This allows SEA to maximize the yield of atomically dispersed gold that is strongly bound to the support without the need of concentrated aqua regia during synthesis. Oxidized gold atoms are known to be the active species for the acetylene hydrochlorination reaction making SEA an ideal synthesis method for catalysts for acetylene hydrochlorination.

1.4 Conclusion

Norit ROX is a steam activated carbon with a surface area of 1225 m^2/g with a point of zero charge of 7.7. Norit was designed for water filtration and is even used in purifying pharmaceuticals so it has superior adsorption properties. If Norit ROX is oxidized it will have far more hydroxyl groups than most carbons due to its high surface area. These two factors allow for Norit to adsorb both gold cations and chloride onto the surface. The chloride that is on the surface can readily adsorb with the Au maintaining a stable $AuCl_3$ or AuCl complex as well as reforming the complex when the HCl is used in the reaction. The $AuCl_3$ and AuCl complexes are actually more stable than metallic gold on the surface of Norit according to DFT studies.[33,34] These superior qualities make SEA of $Au(en)_2Cl_3$ on Norit ROX an ideal candidate for a stable and active catalyst for acetylene hydrochlorination. In this same line of thinking SEA of $Au(en)_2Cl_3$ was theorized to be an ideal way to make Au nanoparticle catalysts on various supports which will be investigated in chapter 2 of this thesis. Preliminary work has also shown that Norit is head and shoulders above other carbon supports for the acetylene hydrochlorination reaction and further study will be done in chapter 3 to explore the reasons why.

Chapter 2

Synthesis of Supported Au nanoparticles by Strong Electrostatic Adsorption of $Au(en)_2Cl_3$

2.1 Introduction

Au nanoparticles have a high potential in catalysis and have been studied extensively for years beginning with Haruta's discovery in 1987 that gold nanoparticles are highly active in CO oxidation reactions at sub-ambient conditions.[35] In 1996 Andreeva et al. reported that gold nanoparticles supported on iron(II) oxide prepared by co-precipitation showed good activity for low temperature water gas shift reaction (WGS).[4] In 1997 Sakuri et al. reported that Au/TiO_2, prepared by deposition-precipitation was active at low temperature for WGS, with an increased Au loading.[36] Gold nanoparticles have also been shown to be catalytically active for several chemical reactions including selective oxidation of hydrocarbons, reduction of NO and acetylene hydrochlorination to form vinyl chloride monomer (VCM).[3] Carbon supported gold catalyst hold great potential for the oxidation of 5-hydROXymethylfurfural into 2,5- furandicarboxylic acid, an important transformation for the production of bio-based polymers. De Jongh et al. have demonstrated that the activity, selectivity, and stability of the carbon-supported gold nanoparticles in the oxidation of 5-hydROXymethylfurfural strongly depend on the surface properties of the carbon support.[37]

In Haruta's work using Au for the oxidation of Co it was found to be difficult to deposit gold via coprecipitation and by deposition-precipitation onto Silica and Al_2O_3 due to the low PZC using $HAuCl_3$, an anionic precursor.[38] The deposition was low and the particles were large, around 20 nm, so Chemical vapor deposition(CVD) was used instead to make small particles. Using CVD 5% Au on Al_2O_3 was obtained with a 3.5 nm particle size. 6% Au on silica was obtained using CVD as well but the size distribution was bimodal and very large. Our use of SEA and $Au(en)_2Cl_3$ has enabled us to reliably deposit small Au nanoparticles on both silica and alumina.

In 2008 Prüße did a study on preparing 0.3% Au on Al_2O_3 catalysts using incipient wetness.[39] This method used $HAuCl_3$ as the precursor and modifying the solution using acids and bases. In this study the catalysts made with 2M HCl performed the best for glucose oxidation. The use of acid to enhance uptake is a similar theory to what is used in SEA but the use of such high concentration is likely to have resulted in low uptake despite Al_2O_3 having a high PZC due to high ionic strength. The 0.3% au on Al_2O_3 were half of the weight loading that we were able to obtain with a similar particle size.

Hutching researched Au on Carbon and TiO_2 using a sol immobilization technique.[40] In this technique colloidal Au was immobilized on the support surface and then treated to remove the scaffolding. This technique resulted in 3.5 nm Au on C and 3.7 nm Au on TiO_2. In another study Hutchings developed a method to produce bimetallic AuPd catalysts with the use of excess Cl^- ions in the incipient wetness technique.[41] During this technique $HAuCl_3$ and $PdCl_2$ are used as salts and HCl is added to the solution in order to promote the formation of $AuCl_4^-$ and $PdCl_2^-$ which can readily deposit onto a protonated surface caused by the HCl.

In this work we demonstrate a simple, scalable synthesis of ultra-small (<2nm) Au nanoparticles on a variety of supports using strong electrostatic adsorption (SEA). SEA is used to create highly dispersed nanoparticles that are strongly bound to a support by controlling the pH of the solution. By controlling the pH of the solution relative to the support point of zero charge, the surface of the support becomes protonated or deprotonated resulting in an electrostatic interaction with an oppositely charged ionic precursor complex. The maximum uptake was used for each respective support is to demonstrate that SEA can produce ultra-small uniform nanoparticles particles at high weight loadings which is difficult for most conventional catalyst synthesis methods. This method is extendable to many other supports with low or mid-range points of zero charge. The use of $Au(en)_2Cl_3$ is significant because there aren't any other viable cationic precursors for SEA onto low PZC supports. The only other option is $(NH_3)_4Au^{+3}$ which is pyrophoric, which means explosive, and dangerous. It is often called fulminating gold. Dry impregnation (DI) will be used to make catalyst of the same weight loading to compare.

Previous work has already been done showing the stability of the $Au(en)_2Cl_3$ salt in solution over time and over a wide pH range. A kinetic study was also done with the adsorption of $Au(en)_2Cl_3$ onto A300 silica and Asbury carbon. It was found that A300 uptakes the gold almost immediately while the pH of the solution changes over the course of 60 minutes which is expected for SEA. Adsorption over Asbury is slow and takes up to 200 minutes to complete while the pH shift happens almost immediately suggesting the possibility of some reductive adsorption mechanism. Surface coverage was found to be 1.2 $\mu mol/m^2$ and was determined by doing uptake surveys at various surface loadings and concentrations to determine, XANES and EXAFS were also performed on various SEA

slurries to determine the coordination number of the gold salt in solution. TPR was done and it was found that 180° C is a temperature where the gold is reduced under a 10% H_2 gas flow for all the catalysts made.

2.2 Experimental

Materials

These experiments employed numerous support materials, which are shown in Table 3.1. SiO_2 (amorphous and mesoporous), γ-Al_2O_3, TiO_2, Nb_2O_5[42], ZrO_2, and graphitic carbon were used directly from the manufacturers. CeO_2 was obtained through calcination of cerium(III) acetate hydrate at 500 °C for 4 hours. Nb_2O_5[27] was achieved by calcination of niobic acid at 500 °C for 2 hours.

Gold bis-ethylenediammine, $Au(en)_2Cl_3$ was prepared as described by Block and Blair.[43] This method involves the dissolving $HAuCl_3$ and ethylene diamine each in ethyl ether followed by the addition of the ethyl diamine in ether solution to the $HAuCl_4$ ether solution slowly. The liquid resulting from the previous step is decanted and the remaining precipitate is dissolved in a small amount of water. The $Au(en)_2Cl_3$ is then precipitated with ethyl alcohol, decanted, redissolved in water again, and precipitated with ethyl alcohol once again. This dissolved $Au(en)_2Cl_3$ is then filtered and left to dry for 2 days covered in at room temperature. With this method we achieved 60% conversion of $HAuCl_4$ to $Au(en)_2Cl_3$. There are other methods utilized for the synthesis of $Au(en)_2Cl_3$. One such method was the dissolution of $HAuCl_4$ and ethylene into water instead of ethyl ether and mixing followed by precipitation with ethanol, filtration, and drying.[44] Figure S1 is XRD pattern obtained to confirm synthesis of $Au(en)_2Cl_3$and its monoclinic crystal structure. The obtained XRD pattern was confirmed by previous work done by Minacheva in 1988.[45]

Table 2.1: Support materials used for experimentation and obtainable weight percentage of metal per support material

Support	Surface Area (m^2/g)	PZC	Wt (%)
Silica			
A90	93	4.2	1.4
A300	330	4.2	5.1
Graphite			
Ashbury	115	5.2	1.7
Mesoporous Silica			
SBA-15	574	4.2	8.2
Titania			
Sach	345	4	5.1
P25	50	4	1
Alumina			
ɣ-Al_2O_3	277	8.4	0.74
Niobia			
Nb_2O_5 (Amorph)	159	2.5	4.3
Nb_2O_5 (Hex)	20	6	0.46
Zirconia			
ZrO_2	22	7	0.3
Ceria			
CeO_2	97	8.4	0.7

Strong Electrostatic Adsorption Survey

Fresh $Au(en)_2Cl_3$ was prepared and dissolved in water at a concentration of 200 ppm across the pH range of 2-13 using HCl or NaOH. The initial pH values were recorded and support material was added to 30 ml of solution at a surface loading of 1000 m^2/L. Samples were then shaken for 1 hour. After 1 hour of contact 10 ml of each sample were filtered and final pH values were measured. A plot was then constructed with pH final vs pH initial. To determine the kinetics involved in this adsorption experiment a set of samples

was also prepared at the optimal adsorption pH, while varying the time $Au(en)_2Cl_3$ was in contact with an amorphous silica support (A300). Both initial and filtered final sample at each pH were analyzed by ICP to determine Au concentration. The surface coverage, or Γ, is calculated from the equation below.

Adsorption data is plotted with the final pH values along the x-axis and gold adsorption along the y-axis as surface density (mol/m^2).

$$\Gamma\left(\mu mol\ Au/_{m^2}\right) = \frac{\left(Conc_{initial} - Conc_{final}\right)\left(\mu mol/_{L}\right)}{Surface\ Loading\ \left(m^2/_{L}\right)}$$

Catalyst Preparation by Strong Electrostatic Adsorption

The synthesis method that will be utilized will be strong electrostatic adsorption (SEA). SEA is the cornerstone method of catalyst synthesis for the Regalbuto research group. This method accounts for the charge of support surface in the adsorbing of solution as a function of pH of the solution. Cationic or anionic metal precursors adsorb onto the surface because of electrostatic interactions between the precursor and the support. Electrostatic interactions are ensured based on the pH of the solution and the oxidation state of the surface. The degree of protonation or deprotonation of the surface hydroxyl groups as a function of adsorbate solution pH determines if there is a driving force for either cationic or anionic precursor to adsorb onto the surface. The pH at which the net charge on the support becomes zero is called the point of zero charge or PZC.

Fresh $Au(en)_2Cl_3$ was prepared at 200 ppm and adjusted to the optimum pH value to obtain maximum surface coverage based off the adsorption survey experiments. Each support was then weighted out for a surface loading of 1000 m^2/L and added to the necessary volume of pH adjusted Au solution. After 1 hour of shaking and contact the solid

support material was filtered and dried at room temperature for 72 hours, due to the thermal degradation of the $Au(en)_2Cl_3$ at temperatures above 50 °C. ICP-OES was used to determine maximum gold uptake.

Catalyst Preparation by Dry Impregnation

Maximum Au surface coverage was determined by the adsorption experiments. Weight percentage based off the maximum uptake was calculated. Each support was then loaded with its respective weight percent by dry impregnation (incipient wetness impregnation). These catalysts were then dried at room temperature for 72 hours to ensure complete drying.

Characterization of Au Supported Catalysts

Analysis of higher weight percent samples, prepared by SEA, was characterized by temperature programmed reduction (TPR) through the use of a Micromeritics Autochem II 2920. 10% H_2/Ar was used at the reductive gas. All were reduced from room temperature to 650 °C at 3 °C/min ramp and H_2 consumption was monitored by thermal conductivity detector. All samples had the equivalent moles of gold present for reduction. Also fresh and aged samples were analyzed.

Scanning transmission electron microscope (STEM) "z-contrast" imagine was performed on a JEOL JEM-2100F 200 kV FEG-STEM/TEM with a digital camera at Aberration-Corrected Scanning Transmission Electron Microscopy Facility, University of South Carolina. It is a 200 kV field emission transmission electron microscope with a Schottky field emission electron source and fitted with an ultra-high resolution pole piece, which in STEM mode is capable of producing a probe size of 0.13 nm with 15 pA of current. Images were taken using both bright field transmission and a high angle annular dark field

detector. Each image was then analyzed using "Particle2.exe" software to determine average particle size as well as standard deviation. Prior to STEM "z-contrast" imaging each sample was reduced under hydrogen flow at 200 °C for 1 hour to ensure complete reduction of gold and removal of any residual ligands.

2.3 Results

$Au(en_2)Cl_3$ adsorption by SEA

Adsorption survey experiments were performed at initial pH values in the range of 2-13. The adsorption solutions were 200 ppm Au in contact with a variety of support materials listed in Table 3.1 at a surface loading of 1000 m^2/L. Results of the adsorption survey experiments and the pH shift experiments are shown in Figure 2.3 a and b respectively. The obtainable weight percentage of Au onto each support is also shown in Table 1.

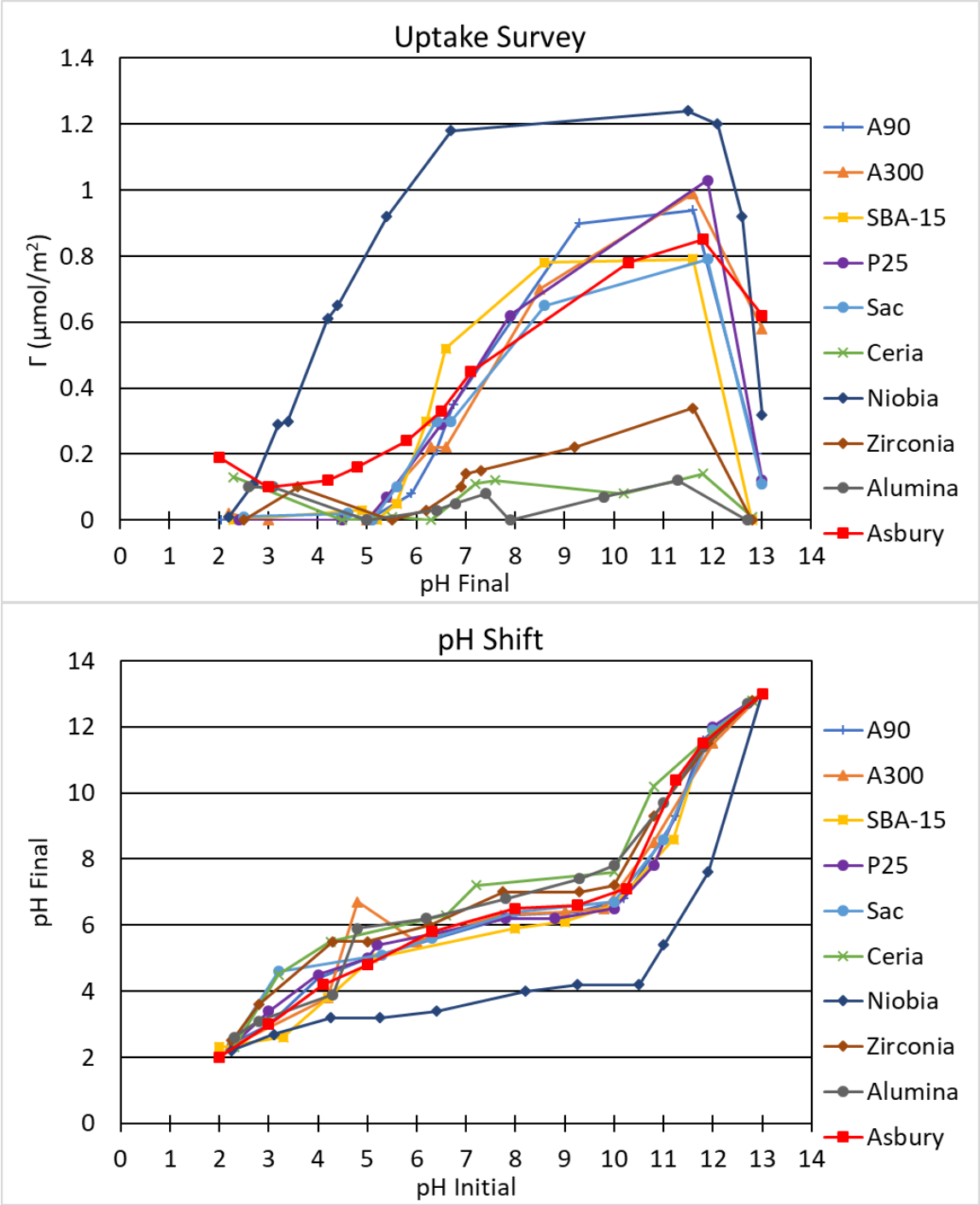

Figure 2.1: Adsorption survey experiments with various support materials and pH shift data for adsorption survey experiments

Overall, all support materials showed the expected strong electrostatic adsorption trends seen in previous work for the adsorption of a cationic complex. Maximum

adsorption was obtained in the basic pH range with retardation of the adsorption at a pH of 13 due to the high ionic strength of the contacting solution.

The high PZC supports (i.e. alumina, ceria, and zirconia) are in agreement with our previous works showing little to no adsorption taking place due to a low density of surface hydroxyl groups being deprotonated in a basic pH environment.[24] Support material with a mid PZC (i.e. silica (amorphous and mesoporous), titania, and graphitic carbon) adsorbed a higher surface coverage of gold because of the an increased density of the surface hydroxyl groups are deprotonated. The lowest PZC support, niobia_159, obtained the highest surface coverage due to an extremely high density of surface hydroxyl groups were deprotonated.

2.4 Catalysis Synthesis and Characterization

XRD spectra were taken in order to determine the average diameter of the gold particle sizes. Catalysts synthesized with SEA were compared with catalysts made using Dry Impregnation for comparison. The spectra are shown in Figure 2.5 Average particle size analysis for the two preparation techniques are shown in Table 3.3.

The silica supports gave the most uniform and smallest particles. The amorphous silicas A90 and A300, as well as the mesoporous silica SBA-15 gave very small and uniform particles even at high weight loading. A300 has a higher surface area than A90 therefore the highest weight loading achieved for A300 was higher than that of A90 yet the Au particle sizes were similar when using the SEA method. SBA-15 has the highest surface area of the Silicas and therefore has the highest maximum weight loading at 8.2% while still maintaining the smallest particle size of all the silicas at 2.4 nm. Background subtraction can easily be done because of the smooth silicon support XRD spectra as seen

in Figure 2.5. Background subtraction using the DI catalyst spectra results in a more accurate deconvoluted spectra because there is a closer intensity and stretching from metal nanoparticle peaks giving a more accurate baseline subtraction than if the support XRD spectra was used.

Table 2.2: Average particle size analysis from STEM and XRD characterization over Au supported catalyst

	Surface Area (m^2/g)	**PZC**	**DI Au (%)**	**DI XRD davg**	**SEA Au (%)**	**SEA STEM d_{avg}**	**SEA XRD d_{avg}**
Silica							
A90	93	4.2	1.4	18.5	1.4	2.6	2.9
A300	330	4.2	5.1	19.7	5.1	2.8	2.4
Graphite							
Ashbury	115	5.2	1.7	19.1	1.4	2.2	2.2
Mesoporous Silica							
SBA-15	574	4.2	8.2	24.4	4.3	2.9	2.4
Titania							
Sachtleben	345	4.0	5.1	27.4	2.2	2.7	1.9
P25	50	4.0	1.0	31.6	1.0	4.7	2.6
Alumina							
ɣ-Al_2O_3	277	8.4	0.74	5.3	0.74	1.7	2.7
Niobia							
Nb_2O_5 (Amorph)	159	2.5	4.3	8.9	4.3	4.2	4.3
Zirconia							
ZrO_2	22	7.0	0.3	17.6	0.3	1.6	<1.5
Ceria							
CeO_2	97	8.4	0.7	24.2	0.7	1.3	<1.5

XRD Characterization

Carbon has been known to be good support for monometallic Au catalysts made with SEA using $Au(en)_2Cl_3$.[46] The graphitic carbon support Asbury with its highly crystalline surface readily electrostatically adsorbs very small uniform Au nanoparticles. The particle size from XRD is 1.6 nm at a weight loading of 1.4%. The XRD pattern in Figure 2.5 d shows a very broad peaks for the Au (111) and Au (200) peaks meaning that the particles are very small. The Au (200) peak is within one of the characteristic graphite peaks but after careful base line subtraction both peaks can be clearly seen and analyzed.

The Au on titania is more difficult than silica or carbon to electrostatically adsorb Au onto the surface. To get adequate surface loading an excess of $Au(en)_2Cl_3$ needed to be added to the solution during synthesis to drive the process forward. In Figure 2.2 c and d you can see the comparison of the XRD of the SEA and the DI samples of Sach titania. The DI Au on titania sample spectra have clear Au peaks because of large particles. The SEA Au on titania catalysts have XRD spectra with no easily visible Au peaks but peaks can be seen after careful background deconvolution.

The average particle size from the XRD spectra of the Au on Nb_2O_5 catalyst is 4.3 nm from the XRD profile in figure 2.2 e. The Nb_2O_5 support is very acidic resulting in a easy adsorption of the cationic precursor when the surface is deprotonated. There is the development of a shoulder of the large Nb_2O_5 peak at 26° for the DI sample but and there is a complete shift in the same peak for the SEA sample of almost 2 degrees. This may be due to the reduction process for the Au nanoparticles carried out at 180 °C in 10% causing the morphology to begin to shift to a more crystalline phase. Amorphous Nb_2O_5 is known to shift to a HCP structure when calcined at elevated temperatures.[47] The Nb_2O_5 used is

amorphous resulting in the Au on Nb_2O_5 catalyst has particles that are small and well dispersed but not very uniform as can be seen in Figure 2.3 e.

The ɣ-Al_2O_3 is a high PZC support with a PZC of 8.4 which naturally results in a lower overall uptake relative to the low PZC supports with similar surface areas. The maximum uptake obtainable is 0.74% which can be deconvoluted from the XRD spectra seen in Figure 2.2 f yielded a particle diameter of 2.7 nm. Both CeO_2 and ZrO_2 are high PZC supports with relatively low surface area resulting in low uptake even in basic solution. Due to the small number of particles and the small size of the particles present neither of XRD spectra could be background subtracted as seen in Figure 2.2 g and h. The CeO_2 support XRD spectra yields a very flat pattern around 38.1° and 44.5° where the Au (111) and Au (200) peaks respectively are which are the most prevalent Au peaks. The XRD instrument used has a detection limit of 1.5 nm so the particles are assumed to be smaller than the detection limit since peaks are not seen.

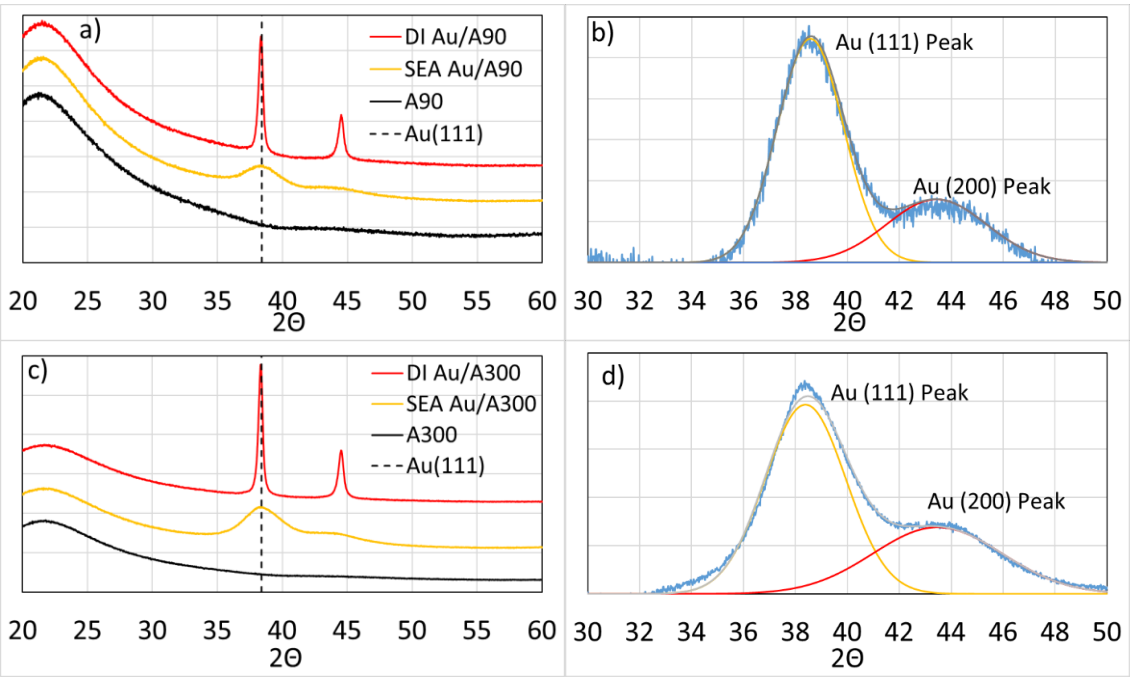

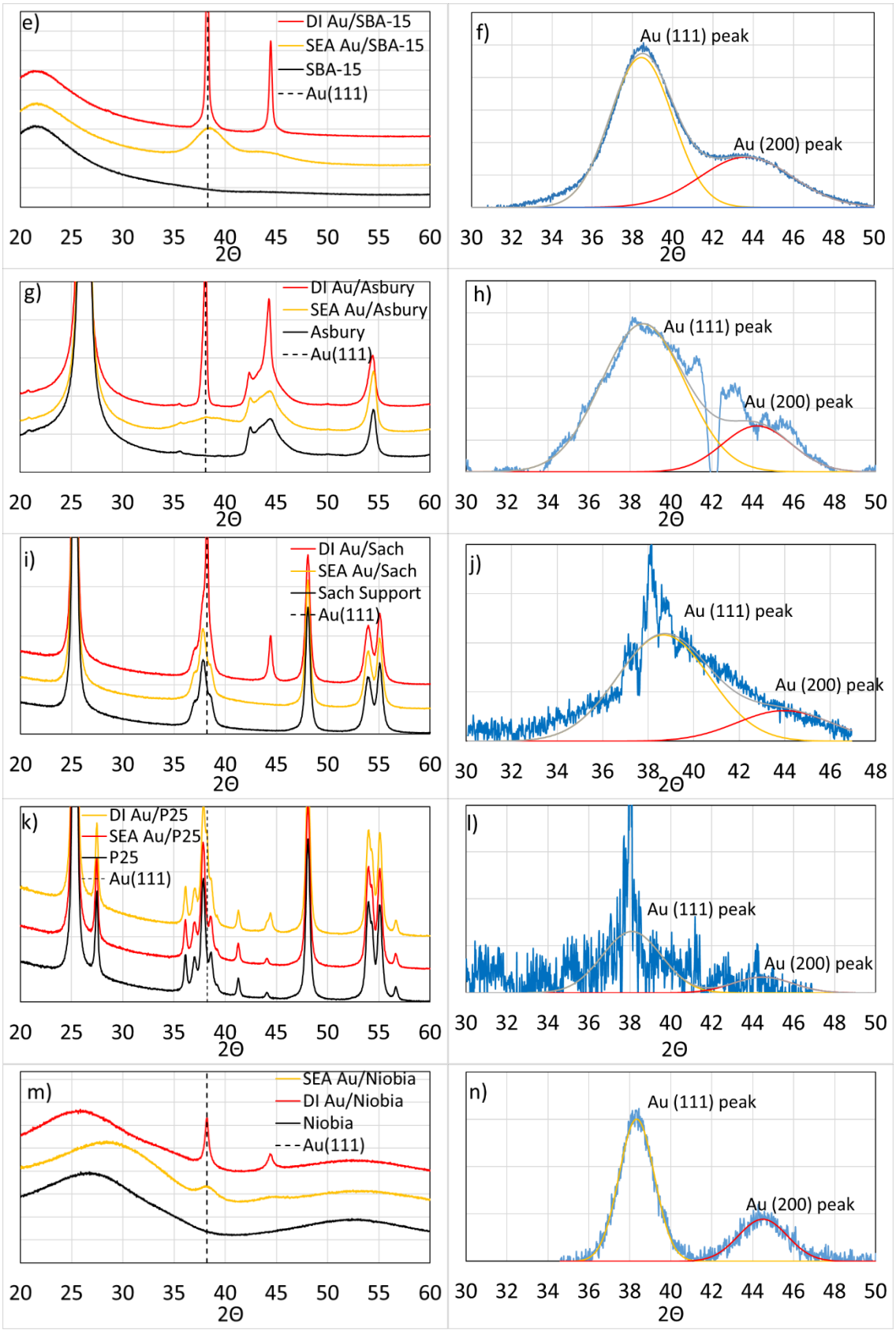
e)
DI Au/SBA-15
SEA Au/SBA-15
SBA-15
Au(111)
20 25 30 35 40 45 50 55 60
2Θ
f)
Au (111) peak
Au (200) peak
30 32 34 36 38 40 42 44 46 48 50
2Θ
g)
DI Au/Asbury
SEA Au/Asbury
Asbury
Au(111)
20 25 30 35 40 45 50 55 60
2Θ
h)
Au (111) peak
Au (200) peak
30 32 34 36 38 40 42 44 46 48 50
2Θ
i)
DI Au/Sach
SEA Au/Sach
Sach Support
Au(111)
20 25 30 35 40 45 50 55 60
2Θ
j)
Au (111) peak
Au (200) peak
30 32 34 36 38 40 42 44 46 48
2Θ
k)
DI Au/P25
SEA Au/P25
P25
Au(111)
20 25 30 35 40 45 50 55 60
2Θ
l)
Au (111) peak
Au (200) peak
30 32 34 36 38 40 42 44 46 48 50
2Θ
m)
SEA Au/Niobia
DI Au/Niobia
Niobia
Au(111)
20 25 30 35 40 45 50 55 60
2Θ
n)
Au (111) peak
Au (200) peak
30 32 34 36 38 40 42 44 46 48 50
2Θ

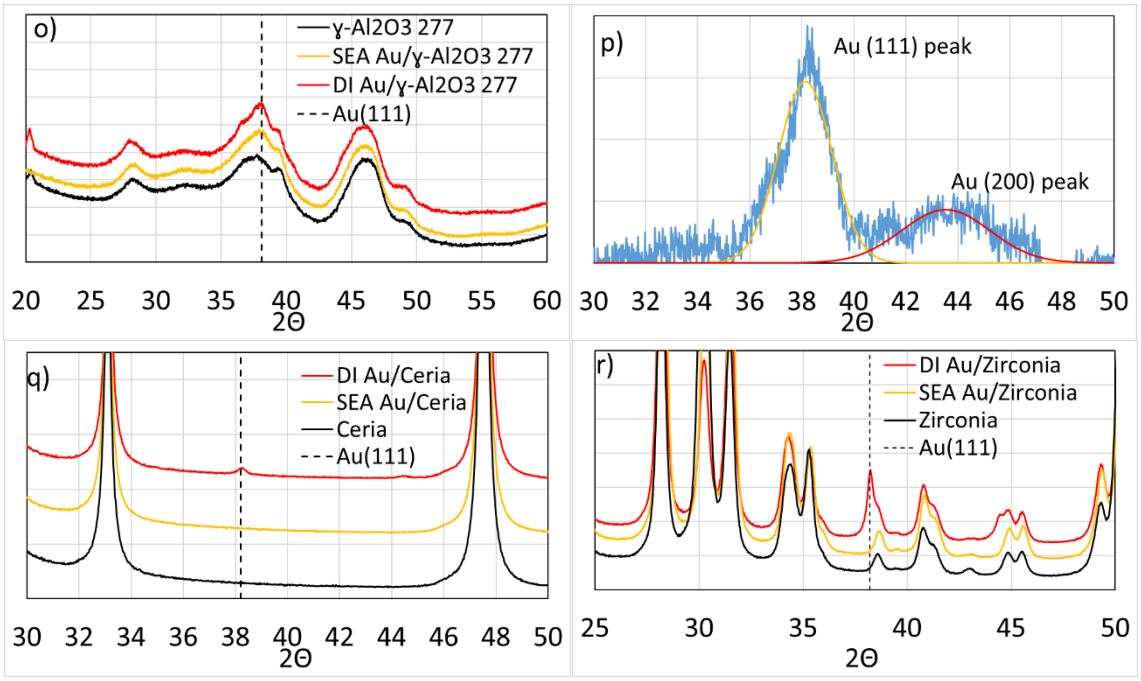

Figure 2.2: XRD of SEA and DI Au on various supports and deconvolution of supported Au on a,b)A90 c,d) A300 e,f) SBA-15 g,h) Asbury i,j) Sachtleben k,l) P25 m,n) γAl_2O_3 o,p) Nb_2O_5 q) CeO_2 and r) ZrO_2

STEM Characterization

Numerous STEM images were taken to make an accurate determination of the average gold particle size. The representative STEM images of selective catalysts and size distribution graphs are shown in Figure 2.3. Particle sizing was done over an average of 1000 particles from a dozen images of each sample when available due to the low weight loading. Average particle size analysis with standard deviations for the two preparation techniques are shown in Table 3.

Each of the catalyst supports maintained an average particle size of 4 nm or below, which is significantly smaller than the DI prepared counterparts. The silica catalysts each show very well dispersed particles with tight size distribution. The SBA-15 catalyst has well distributed particles even inside the long narrow pores that are characteristic of this silica. It is very difficult to get particles to form throughout the pores of SBA-15 using the

DI method because of transport limitations and particle sizes. The Asbury carbon catalyst shown in Figure 2.6 d has small well distributed Au particles. The average particle size from STEM of 2.1 nm shows a slight discrepancy with the size calculated from XRD of 1.6 nm. The amorphous Nb_2O_5 catalyst has well distributed particles but there is a wide size distribution as seen in the STEM image and size distribution graph in figure 2.3 f. This wide size distribution may be due to the acidic nature of the support. The ɣ-Al_2O_3 catalyst shown in Figure 2.3 g consists of ultra-small nanoparticles with a small amount of large agglomerations.

The mean particle size of the Au on Sachtleben TiO_2 is 2.7 nm from analysis of the STEM images. The images show that there is a bimodal size distribution consisting of a majority of small nanoparticles with a small amount of larger particles above 4 nm. A mean particle size of 2 nm had been seen previously on titania (P25) at a reduction temperature of 200 °C at a slow heating rate (1 °C/min), and another P25 sample reduced at 300 °C at the same heating rate produced virtually the same particle size. This comparable average particle size could involve the reduction of the titania support, which would hinder the sintering of the Au nanoparticles at an elevated temperature.[42,48–50]

Due to low weight loadings and lack of Z contrast due to similar atomic weights it is difficult to see particles on CeO_2. The ZrO_2 catalyst has very small particles with a tight size distribution but due to the low weight loading the particles are not closely packed.

Overall, samples prepared by SEA produced a smaller average particle size with a narrow standard deviation, while samples prepared by traditional dry impregnation produced larger particles with higher standard deviations, especially on the amorphous silica supports. This increase in particle size is due to a lack of a strong precursor-support

interaction. When dry impregnation is used the surface of the support is neutrally charged or at the PZC and a lack of attractive force prevents the metal complex from being properly anchored, leading to an increase in average particle size and standard deviation.

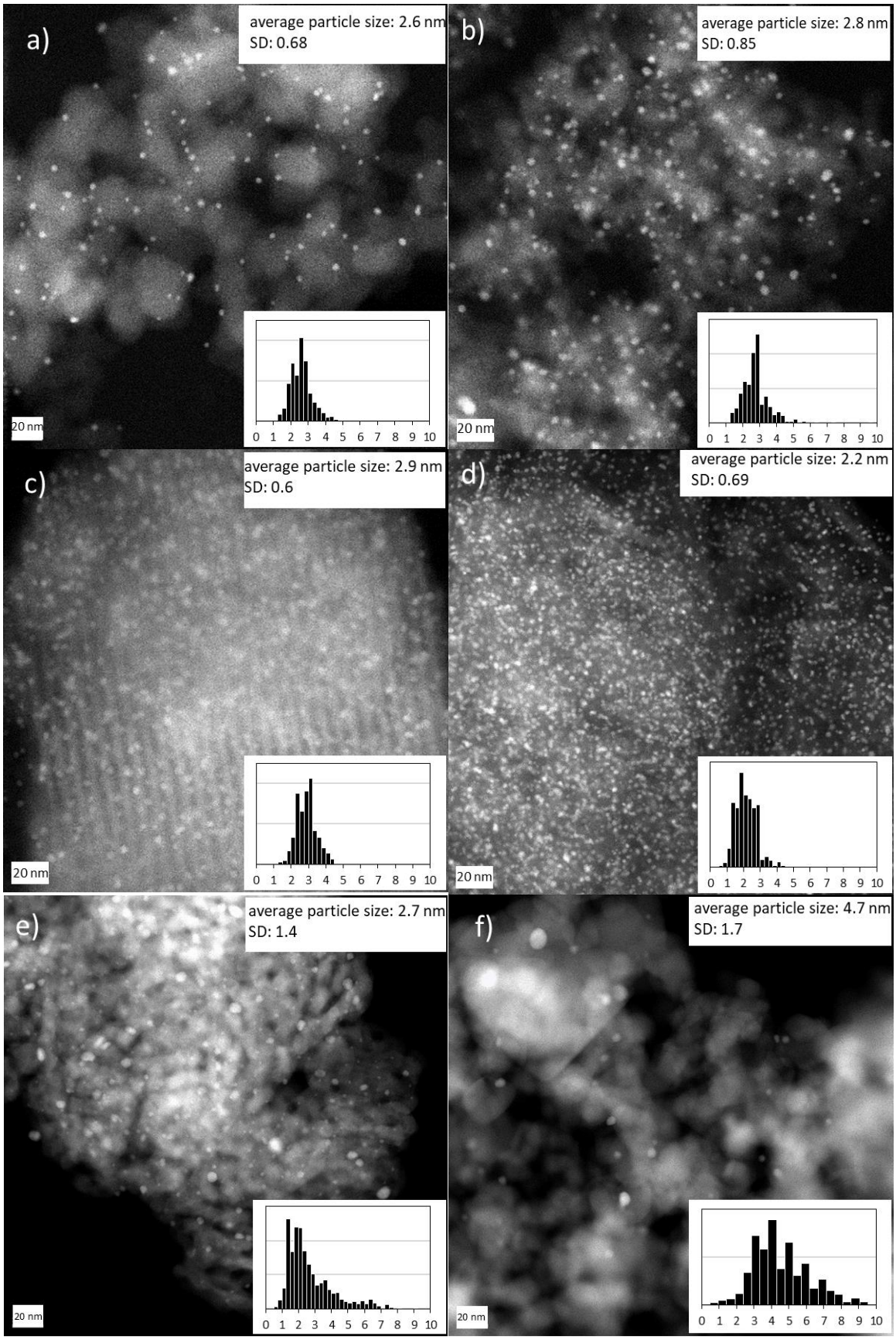
a)
average particle size: 2.6 nm
SD: 0.68
20 nm
0 1 2 3 4 5 6 7 8 9 10
b)
average particle size: 2.8 nm
SD: 0.85
20 nm
0 1 2 3 4 5 6 7 8 9 10
c)
average particle size: 2.9 nm
SD: 0.6
20 nm
0 1 2 3 4 5 6 7 8 9 10
d)
average particle size: 2.2 nm
SD: 0.69
20 nm
0 1 2 3 4 5 6 7 8 9 10
e)
average particle size: 2.7 nm
SD: 1.4
20 nm
0 1 2 3 4 5 6 7 8 9 10
f)
average particle size: 4.7 nm
SD: 1.7
20 nm
0 1 2 3 4 5 6 7 8 9 10

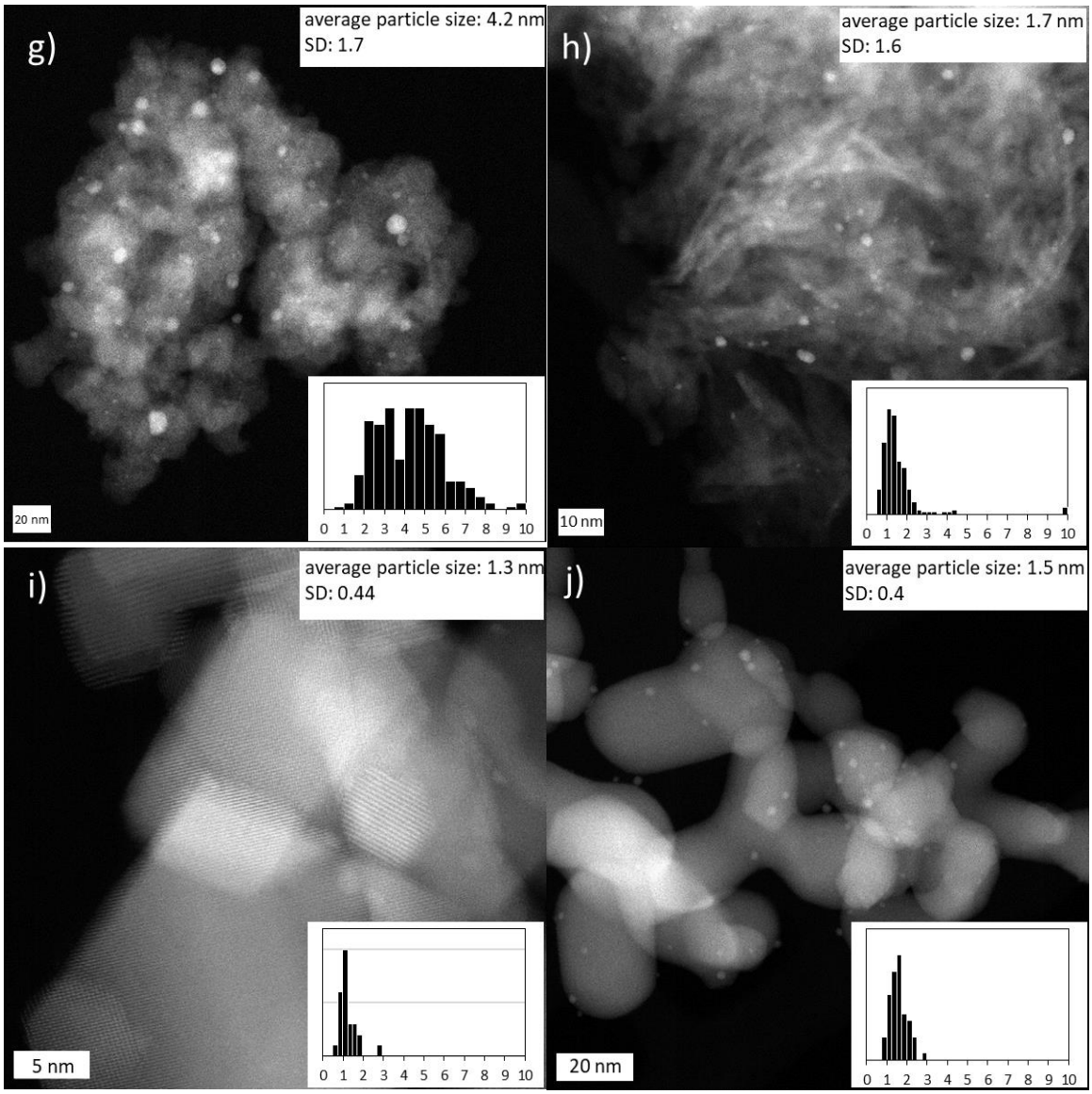

Figure 2.3: STEM images and corresponding particle size analysis of SEA Au on a) A90 b) A300 c) SBA-15 d) Asbury e) Sachtleben f) P25 g) Al_2O_3 h) Nb_2O_5 i) CeO_2 and j) ZrO_2

2.5 Discussion

Speciation of $Au(en)_2Cl_3$ in solution

Ethylenediammine can exist in aqueous solutions as three different forms: EnH_2^{+2}, EnH^+, En. Using the equilibrium constants presented in Asku et al.[51] a speciation plot can be modeled and is shown in Figure 2.7. From the speciation curves it is clear that at a pH lower than 7 a doubly protonated ethylenediammine (EnH_2^{+2}) is the dominate species,

while ethylenediammine (En) dominates in a basic environment starting around a pH of 9. The intermediate pH values are dominated by the singly protonated ethylenediammine (EnH^+). This model was confirmed by experimental work exploring the protonation and deprotonation En.[51–53] This data shows that En is basic in nature and readily gives up excess hydrogen.

The EXAFS results revealed that $Au(en)_2Cl_3$ changed to a trigonal planar geometry with increasing pH. Prior work has explored speciation and complexation of $Au(en)_2Cl_3$ in acid and alkali solutions.[43,53] These works state that as the hydrogen ion concentration decreases in solution, one of the ethylenediammine ligands will deprotonate releasing a hydrogen ion into solution.

Speciation curve of $Au(en)_2Cl_3$ was constructed using the equilibrium constants calculated from spectroscopic data from previous work. The results of this modeling are shown in Figure 2.7. Figure 2.7 a illustrates that formation of $[Au(En)(En\text{-}H)]^{2+}$ begins at a pH of 6 and at a pH of 10 $Au(en)_2Cl_3$ has changed entirely to this deprotonated ethylenediammine Au complex. This is consistent with Figure 7 b which shows that a drop in the coordination number from a pH of 6 to pH of 10, where the coordination number of $Au(en)_2Cl_3$ is approximately 3. From these results it can be suggested that $[Au(En)(En\text{-}H)]^{2+}$ has the trigonal planar geometry illustrated in Figure 2.4 c. The hydrogen released from the ethylenediammine is on the nitrogen group bound to the gold center. In previous work this release of hydrogen was a result of a charge transfer affect, which resulted in a shift of a UV band that was not present when the complex was dissolved in water.[54]

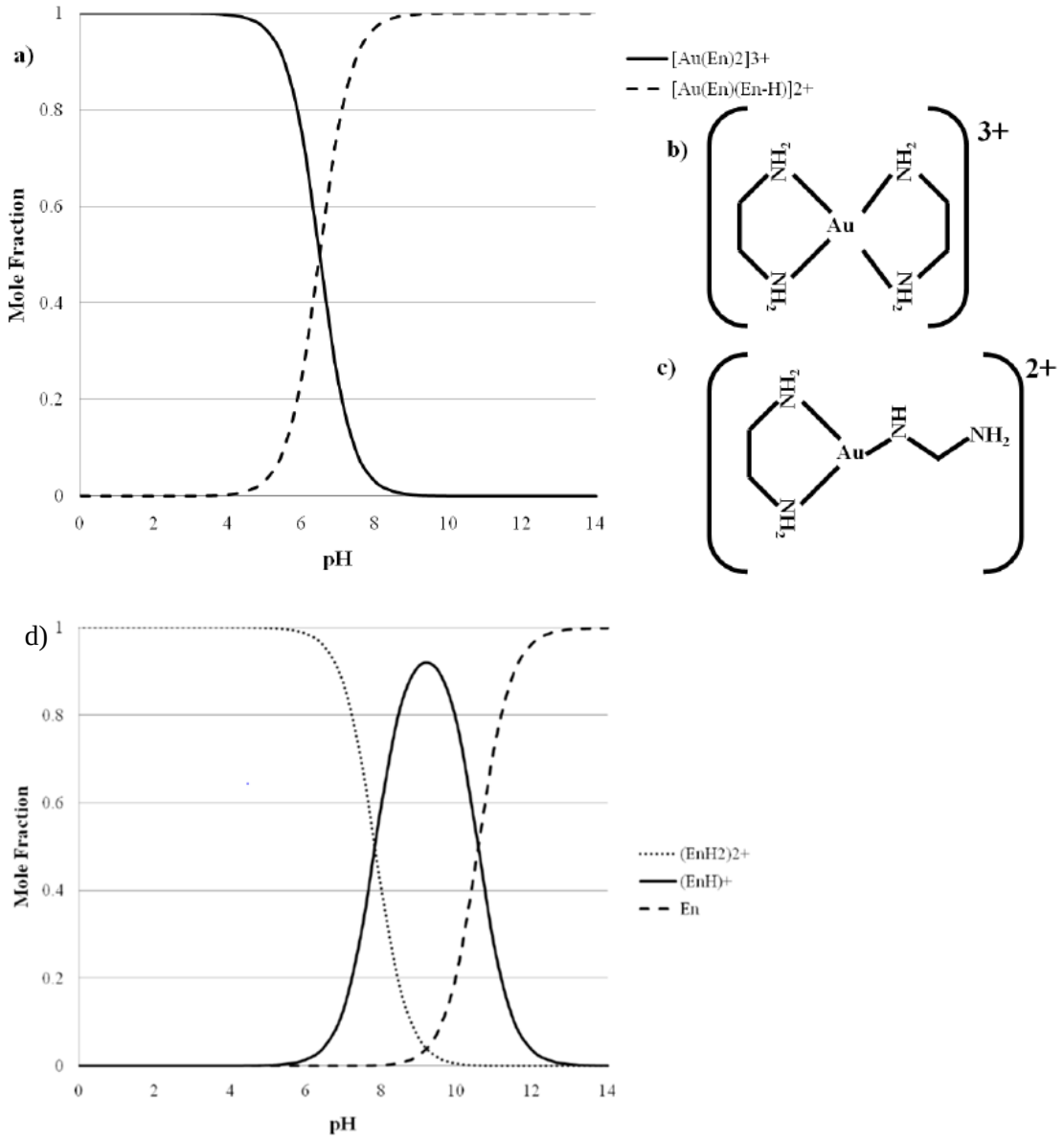

Figure 2.4: a) Speciation curves of ethylenediammine in aqueous solution, b) structure of $Au(en)_2Cl_3$ in solution at pH below 6, c) postulated $[Au(En)(En\text{-}H)]^{2+}$ complex, and d) Speciation curve of $Au(en)_2Cl_3$ in aqueous solution ($[Au(en)_2]^{3+}$= $Au(en)_2Cl_3$ in solution, $[Au(En)(En\text{-}H)]^{2+}$=deprotonated ethylenediammine Au complex)

Also, at acidic pH values the complex underwent another structural change but with chlorine. The presence of 2 Au-Cl with 2 Au-N backscatters was evident on both the fresh and aged samples. Previous research involving the interaction of $Au(en)_2Cl_3$ with chloride

ions showed that a substitution of ethylenediammine with chlorine ions would take place when excess chlorine was present in solution.[55] Based off the results of the EXAFS and prior work it can be assumed that at very acidic pH using HCl as the acid would allow $Au(en)_2Cl_3$ to undergo a substitution of one of the ethylenediammine ligands with chlorine. From all of the above assumptions a series of reactions can be designed to show the possible speciation of $Au(en)_2Cl_3$ with increasing pH:

Reaction 1: Acidic Conditions

$$[Au(en)_2]^{3+} + 2H^+ + 2Cl^- \leftrightarrow [Au(en)Cl_2] + enH_2{}^{2+}$$

Reaction 2: Basic Conditions

$$[Au(en)_2]^{3+} + Na^+ + OH^- \leftrightarrow [Au(en)(enH)]^{2+} + Na^+ + H_2O$$

Besides the change in coordination number there was an increase of the Au^0 fraction as the pH of the gold solutions were increase. After samples were analyzed at the APS there was an apparent red hue to the solution. The red color of the solution is typical of metallic gold.[56] However, since there was no evidence of Au-Au bonds present in the EXAFS fitting it can be hypothesized that the formation of reduced gold in solution is very slow if the solution is keep below a pH of 5. It can also then be concluded that with increased oxygen concentration in solution at basic pH the possibly of the formation of reduced gold is increased.[57]

2.6 Conclusion

From the stability study of $Au(en)_2Cl_3$ it can be concluded that the complex is stable below a pH of 5 at least for one month. The complexes undergo a structural change from square planar to trigonal planar as pH is increased past 7. We suggest that this occurs as a hydrogen ion from the nitrogen group close to the Au center is released while the other

nitrogen group breaks away from the Au center forming an ethylenediammine tail and a drop in oxidation state occurs. An increase in the metallic gold fraction occurred with increased concentration of hydroxide concentration.

The SEA method has been extended to the preparation of supported metal catalysts using this cationic gold complex. The mechanism of adsorption over a silica support is electrostatic in nature, while adsorption over a carbon support shows signs of an additional reductive mechanism. Evidence of a reductive mechanism on carbon is evident from the XAS results of the slurry samples at the optimal pH conditions, which showed increased metallic gold fraction compared to the solution experiments. The maximum adsorption experiments in conjunction with the XRD pattern of $Au(en)_2Cl_3$ showed that one hydration sheath is retained as the complex is adsorbed. Modeling of adsorption on silica compared to experimental adsorption data suggests that $Au(en)_2Cl_3$ can adsorbs as a +2 complex at high pH.

Catalysts prepared using $HAuCl_4$ tend to have particle sizes twice those prepared with $Au(en)_2Cl_3$. This is probably due to hydrolysis of $HAuCl_4$ in solution leading to a high metal loading being adsorbed with a high amount of sintering taking place. SEA prepared samples compared to the other preparation techniques have comparable average particle sizes at low weight loadings. The DPU prepared samples are capable of producing approximately the same particle size but at significantly higher weight loadings. [58–67]

Chapter 3

Why Norit ROX Rocks

3.1 Introduction

Vinyl chloride monomer (VCM) is the largest produced commodity chemical by volume with a production of over 50 million tons a year. VCM is the monomer used to make polyvinyl chloride (PVC) which is one of the top three plastic polymers produced per year by volume. Due to the volatility in the prices of oil and natural gas, coal derived feedstocks are much more attractive in the commodity chemical world due to low cost and long-term stability. Acetylene is one of these feedstocks and is utilized in the production of VCM via the acetylene hydrochlorination process in places like China due to its abundance of coal. Traditionally the catalyst used for this process is 10-15% mercuric chloride on carbon catalyst and due to the environmental impacts of mercury it will be no longer be used after 2022.

Several nonmercury alternative catalysts have been synthesized and tested with little success.[17,18,68,69] The most promising alternative catalyst is an Au supported on carbon catalyst where the active site is atomically dispersed Au oxidized into the Au(I) or Au(III) state.[12,70] Only carbon supported Au has been shown to be active catalysts for this reaction but Au nanoparticles on carbon supports sinters under reaction conditions.[46] Even among carbon supports there is a significant difference in catalyst activity and stability when using

the various carbons. The leading researcher in this field, Hutchings, primarily used Darco in his early papers but switches to using Norit ROX carbon exclusively after his papers written in 2013.[14,71–73] Since then Norit ROX has been the carbon of choice for most research done in this field. Work has been done at the University of South Carolina by Kerry O'Connell on the relationship between the stability of Au nanoparticles and support used. In this study catalysts made by strong electrostatic adsorption (SEA) of $Au(en)_2Cl_3$ on several carbon and noncarbon supports were analyzed. The Au nanoparticles on noncarbon supports is more stable but inactive. The carbon supported Au catalysts are active but sinter rapidly in the presence of HCl. The most active support was found to be oxidized VXC-72 hinting that the hydroxyl group content on carbon has a major effect on stability and activity.[46] Norit was not used in this study but it is evident that the catalysts in that study were less active and stable than those made with Norit.

Work has been done to modify the Norit carbon surface and to eliminate the use of Aqua Regia in the synthesis process. Nitrogen doped Norit has been shown to be very effective in stabilizing atomic Au and maintaining dispersion under reaction conditions but suffers from deactivation due to pore blockage.[74] Dry impregnation using ionic liquids has been used on the surface of Norit in order to help dispersion and stabilize the oxidized Au nanoparticles and increase the adsorption of acetylene and HCl onto the surface of the Au.[19–21] Activated carbon fibers were compared to Norit as an alternative support for acetylene hydrochlorination.[75] This study utilized temperature controlled desorption to determine which surface oxidation groups were on each of the carbon supports and which groups were binding sites for Au. While the phenol and carbonyl groups on the carbon

fibers were the primary binding site for Au the carboxylic, ether, and carbonyl groups were the primary binding sites on Norit.

In this work we will characterize monometallic carbon supported Au catalysts with powder XRD and XPS. The catalysts will be synthesized via SEA of $Au(en)_2Cl_3$.[24,32] This method allows for metal precursors to be strongly adsorbed onto support surfaces with high dispersion resulting in small particle sizes and even atomic dispersion in some cases. The various carbon supports were oxidized in either different concentrations of HNO_3 or Aqua Regia before deposition of Au in order to modify the point of zero charge (PZC) on the support allowing for better uptake with SEA. Oxidation of the support results in an increased amount of carboxyl groups on the surface of the support which can affect the activity of the catalyst and increase adsorption for SEA.[37] Nanoparticle stability is tested in a He/HCl mixture as well as in acetylene hydrochlorination reaction mixture of $He/HCl/C_2H_2$. When deposited onto Norit carbon Au is atomically dispersed and is stable against sintering in the He/HCl environment. In this study XRD and XPS were performed on different catalysts after synthesis, reduction, and pretreatment in order to elucidate the difference between the Norit carbon and other carbons for this reaction.

3.2 Experimental

Catalyst preparation

One weight percent Au supported on carbon catalysts used in this study were synthesized by SEA of bis(ethylenediamine)gold(III)chloride, $Au(en)_2Cl_3$. The $Au(en)_2Cl_3$ precursor was prepared using the method developed by Block and Bailar.[43] The carbon supports that were used were Norit ROX, Timrex, and VXC-72. The supports were oxidized by refluxing the support in acid at 85° for 1 hour. Each carbon support was

oxidized using HNO_3 or aqua regia of concentrations 15.7 M, 1 M, and 0.5 M. After refluxing for an hour, the supports were washed of residual acid and filtered until the filtrate reached a pH above 4.5 and then dried overnight in an oven. The PZC of each support will then be determined by a 3-point PZC measurement.

Following the determination of the PZC uptake surveys of Au from an $Au(en)_2Cl_3$ precursor were performed. The surface loadings of the carbon were maintained at 1000 m^2/L. A pH shift was performed on each of the carbon supports to estimate the pH in which the highest amount of metal uptake will occur. For each support the optimal uptake occurs around a final pH of 12 so all SEA of done at this pH.

Catalyst characterization

XRD was used on both the fresh and spent samples to observe changes in metal particle size. The XRD instrument is a Rigaku MiniFlex II equipped with a D/teX silicon strip detector and uses Cu Kα radiation. Background subtraction was used to isolate the Au (111) peaks in order to calculate the particle size using the Debye-Scherrer equation.

X-ray photoelectron spectroscopy (XPS) investigation of untreated and treated catalysts was carried out using a Kratos AXIS Ultra DLD XPS (Kratos Analytical). The XPS system is equipped with a monochromatic Al Kα source operated at 15 keV and 150 W , a hemispherical analyzer, charge neutralizer, catalysis cell, and a load lock chamber for rapid introduction of samples without breaking vacuum. The X-rays were incident at an angle of 45°, with respect to the surface normal. Analysis was performed at a pressure of $\sim 1 \times 10^{-9}$ mbar and high-resolution core level spectra were measured with a pass energy of 40 eV. The XPS experiments were performed by using an electron beam,

directed on the sample, for charge neutralization. The curve fitting procedure was carried out using the XPS Peak 41 software and the peak approximation was carried out by a combination of Gaussian - Lorentzian functions, with subtraction of Shirley-type background.

Catalyst evaluation

Hydrochlorination of C_2H_2 was performed using a fixed bed, Pyrex^{TM} reactor (3/8" OD). Prior to the start of the reaction 120 mg of catalyst undergoes a pretreatment with 11 SCCM HCl and 10 SCCM He for 30 minutes at 180° C. Acetylene is then added to the feed containing the pre-chlorided catalysts at a 1:1:1.1 ratio of He:C_2H_2:HCl with a total flow of 31 SCCM. All gas flows were controlled by mass flow controllers (Brooks 5850E). The conversion of C_2H_2 was determined analyzing the C_2H_2 flow from the feed and product stream by a HP 5890 Series gas chromatograph (GC) equipped with a flame ionization detector.

3.3 Results

Three different series of oxidized carbon supports consisting of Norit ROX, Timrex, and Vulcan XC-72 were used for this study using. Each carbon was oxidized in 15.7M, 1M, and 0.5M of both HNO_3 and aqua regia to obtain a variety of different supports with different points of zero charge (PZC). PZC is the pH in solution of a support at which the hydroxyl groups on the surface of the support are neutrally charged. At the pH above the PZC a support is negatively charged and can strongly adsorb positively charged ions. The purpose of oxidizing the carbon supports is to increase the number of hydroxyl groups on the surface of the support and decrease the PZC making it easier to adsorb the positively charged $Au(en)_2^{3+}$ ion for SEA. Table 3.1 shows the various PZC carbon supports obtained

from oxidation. The surface areas of the Norit ROX, Timrex, and VXC-72 are 1225 m^2/g, 280 m^2/g, and 254 m^2/g respectively. Uptake surveys were done on the VXC and Norit series as shown in Figure 3.1. As you can see the uptake increases with decreasing PZC as predicted by the RPA model. [31,76,77] The maximum uptake on 3 PZC VXC-72 is 0.85 $\mu mol/m^2$ which is the equivilent of 4 wt% Au. The maximum uptake on 2.7 PZC Norit ROX is 0.54 $\mu mol/m^2$ which equates to 11.6 wt% Au. This difference is due to the Norit ROX having more surface area than VXC-72 so although the uptake was lower the maximum wt% from one cycle of SEA was higher.

Table 3.1:PZC and surface area of oxidized carbon supports

	Norit	Timrex	VXC-72
surface area (m^2/g)	1225	280	256
no oxidation	7.7	5.4	8
15.7 M HNO3	2.7	2	3
1 M HNO3	4.7	3	4.2
0.5 M HNO3	5.7	4.4	5.2
15.7 M AR	2.5	2	3
1 M AR	5.7	3	4.4
0.5 M AR	6.2	4.4	5.5

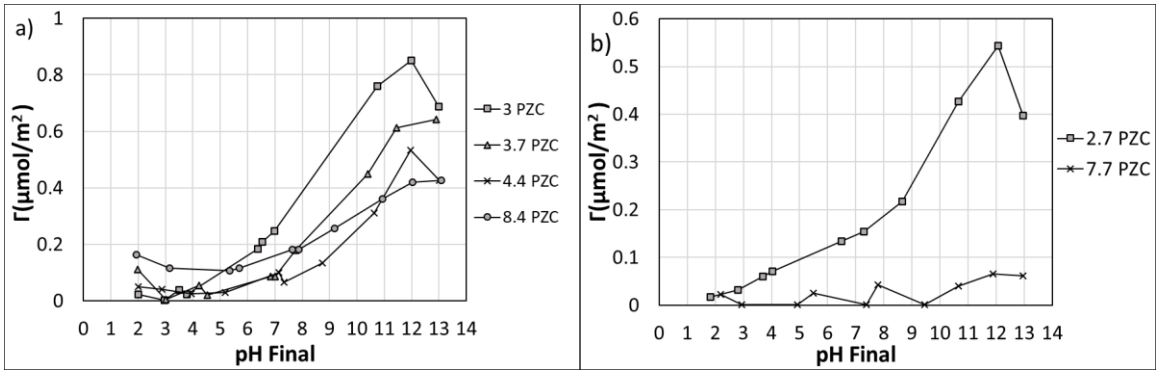

Figure 3.1: Uptake survey of $Au(en)_2Cl_3$ on HNO_3 oxidized a) VXC-72, b) Norit ROX

XRD and XPS characterization

XRD spectra were taken in order to determine the average diameter of the gold particles. The catlaysts were analyzed fresh, after pretreatment, reduced, reduced pretreated, and post reaction as shown in table 3.2 below.

When analyzing the XPS patterns of the samples the Au 4f and Cl 2p regions are of interest because the Au 4f region shows the oxidation state of the Au during and before pretreatment and the Cl 2p region confirms that the oxidized Au is bonded to Cl. In Figure 3.3b and 3.4b the unreduced sample of 1% Au/5.7 PZC AR oxidized Norit show both Au^0 and Au(III), thought to be $AuCl_3$, present from both the Au 4f and Cl 2p regions showing that much of the Au is already oxidized upon deposition. The Au(III) is present because gold cation used in SEA is $Au(en)_2^{3+}$ and the Au maintains that charge upon adsorption. In the XRD pattern in Figure 3.2b for this sample there is no visible Au peak suggesting that the Au in atomically dispersed or in ensembles with sizes below the limit of detection. After pretreatment the relative intensity of the Au(III) to Au^0 in the Au 4f region increases showing that more Cl is being adsorbed onto the Au. The XRD pattern still shows that the Au is atomically dispersed. Upon reduction of the initial sample there are shifts the XPS patterns. In the Au 4f region the peak for Au(III) disappears and instead a small Au(I) peak is present at a lower intensity. Additionally, the Cl peak in the Cl 2p region shifts to the right possibly showing a dissociation with Au. The XRD pattern shows small 3.6 nm metallic Au particles. Upon pretreatment of the reduced catalyst there is a reemergence of the Au(III) peak and a pattern that looks similar to the unreduced pretreated sample. In the Cl 2p region the Cl peak once again shifts left back original position. The XRD pattern for

the reduced pretreated sample once again shows no visible metallic Au peak showing a redispersion of the Au.

Table 3.2: XRD particle sizes of Au catalysts

	Unreduced	Unreduced Pretreated	Reduced	Reduced Pretreated
1% on 4.7 PZC Norit ROX HNO_3 oxi	11.4	10.8	3.5	15.8
1% on 5.7 PZC AR oxi	0	0	3.6	0
1.15% on 3 PZC Timrex HNO_3 oxi	13.8	22.7	9.2	14.7
1.2% on 3 PZC Timrex AR oxi	13.0	17.9	7.3	20.1
0.8% on 7.7 PZC Norit ROX	0	0	3.9	0
1.15% on 4.2 PZC VXC HNO_3 oxi	0	10.4	2.7	8.1
0.9% Au on 3 PZC KBM	10.2	17.9	11.9	20.1

The 1% Au on 4.7 PZC HNO_3 oxidized Norit catalyst is different because the oxidation of the support was carried in HNO_3 which better at oxidation resulting in a lower PZC. The Au 4f region of XPS pattern in Figure 3.3a for the unreduced catalyst shows a small amount of Au(III) compared to Au^0. The XRD pattern in Figure 3.2a shows a small peak corresponding to 11 nm Au. Upon pretreatment the Au 4f region of the XPS shows an increase in the intensity of the Au(III) peak while the XRD stays relatively unchanged showing 11 nm particles. When the catalyst is reduced there is a change in the XPS pattern in the Au 4f region where the Au(III) peak decreases and the Au^0 peak increases showing that more Au was reduced. The XRD pattern for the reduced catalyst shows a huge increase in peak area, displaying a bimodal size distribution, and decrease in average particle size to 3.5 nm. When this sample is pretreated the peak area of the XRD pattern decreases and the particle size of the remaining large particles is 16 nm. The peak area is roughly 8 times

smaller for the reduced pretreated sample compared to the reduced sample showing that most of the particles are redispersed during pretreatment. The Au 4f region of the XPS pattern of this catalyst shows a large decrease in the Au^0 peak intensity and large relative amount of Au(III) to Au^0 as well.

The 1% Au on 3 PZC HNO_3 oxidized Timrex showed the expected XPS and XRD patterns that are typical of Au/C catalysts for this reaction. The XPS of the unreduced sample showed a small amount of Au(III) in both the Au 4f and Cl 2p regions in Figures 3.3c and 3.4c. The XRD showed a small amount of relatively large particles of 14 nm in Figure 3.2c. This small peak area indicates that a majority of the Au is below the detectable limit of the XRD possibly atomically dispersed. Upon pretreatment there is only metallic Au present in the XPS spectra. The XRD shows an 8 fold increase in the peak area of the Au[111] peak and an increase in the average particle size to 23 nm. This sintering of Au in the presence of HCl shows that the atomic Au is not stable on Timrex. When the catalyst is reduced after synthesis the XPS spectra shows only metallic Au and the XRD shows a slight change in particle size to 9 nm and a doubling of peak area. Much of the dispersed Au is reduced and particles as expected. When the reduced catalyst is pretreated the XPS spectra does not change and only metallic Au is seen. The XRD shows a particle size of 14 nm and an increase in peak area even larger than that of the unreduced pretreated sample.

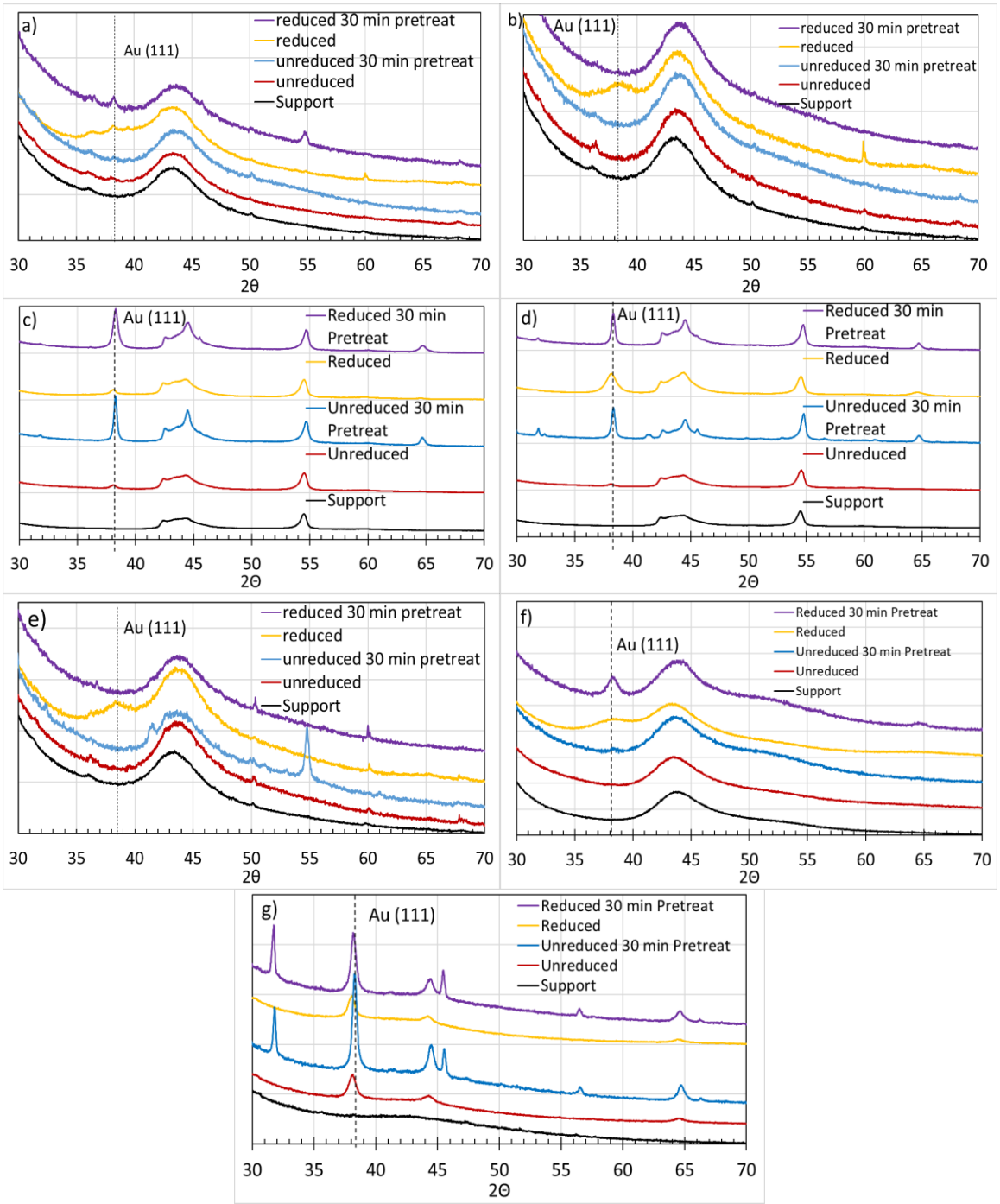

Figure 3.2: XRD of 1% Au on a) 4.7 PZC Norit ROX HNO_3 oxi, b) 5.7 PZC Norit ROX AR oxi, c) 3 PZC Timrex HNO_3 oxi, d) 3 PZC Timrex AR oxi, e) 7.7 PZC Norit ROX f) 4.2 PZC VXC-72 HNO_3 oxi, g) 3.5 PZC KBM

In Figure 3.2d the XRD patterns for the 1% Au on AR oxidized Timrex are shown.

They are similar to the HNO_3 oxidized except when the support is reduced when there is a

large increase in peak intensity and area relative to the unreduced sample. The XPS spectra of this sample in Figure 3.3d and 3.4d show that pretreatment after reduction results in a small amount of Au(III) even though the XRD pattern shows an increase in particle size. This corresponds with the decrease in peak area suggesting a small amount of redispersion at the same time as sintering.

This large difference in pretreated samples suggests that there are more binding sites on Norit ROX than Timrex. This binding site is even more stable than Au-Au bonds suggested by the redispersion of the reduced Au/Norit samples. These binding sites would be hydroxyl groups and defect sites on the carbon surface.

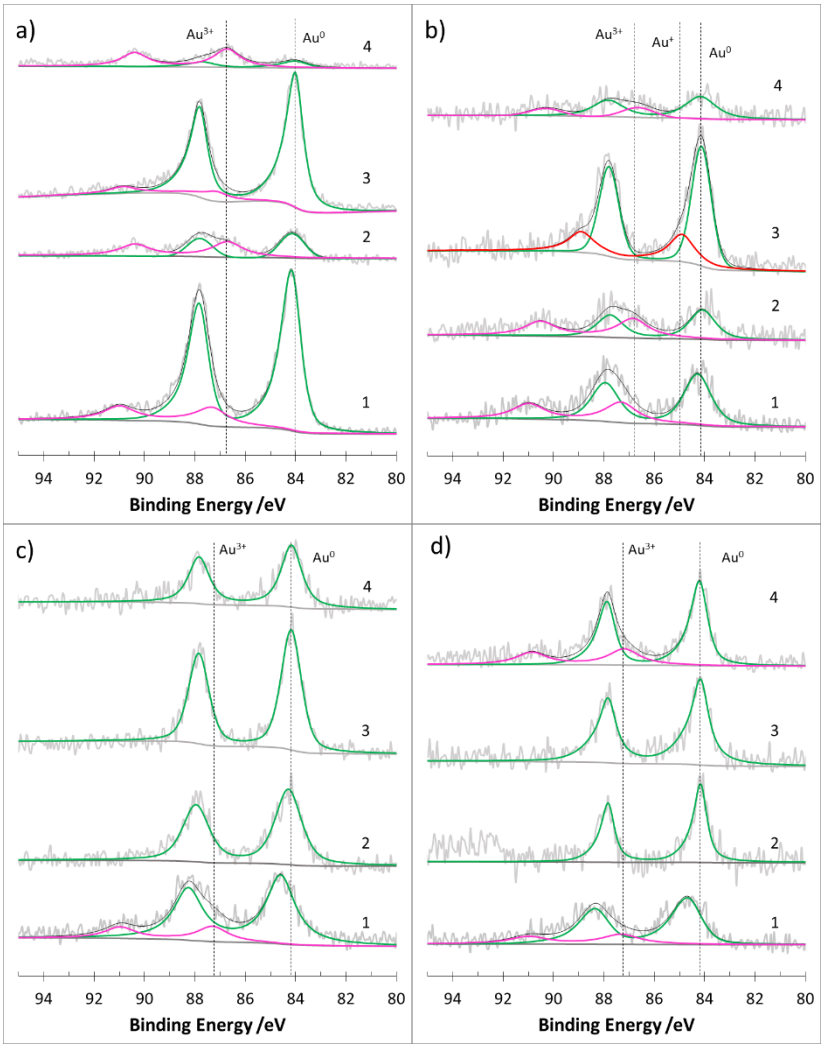
a)
Au3+
Au0
4
3
2
1
94 92 90 88 86 84 82 80
Binding Energy /eV
b)
Au3+
Au+
Au0
4
3
2
1
94 92 90 88 86 84 82 80
Binding Energy /eV
c)
Au3+
Au0
4
3
2
1
94 92 90 88 86 84 82 80
Binding Energy /eV
d)
Au3+
Au0
4
3
2
1
94 92 90 88 86 84 82 80
Binding Energy /eV

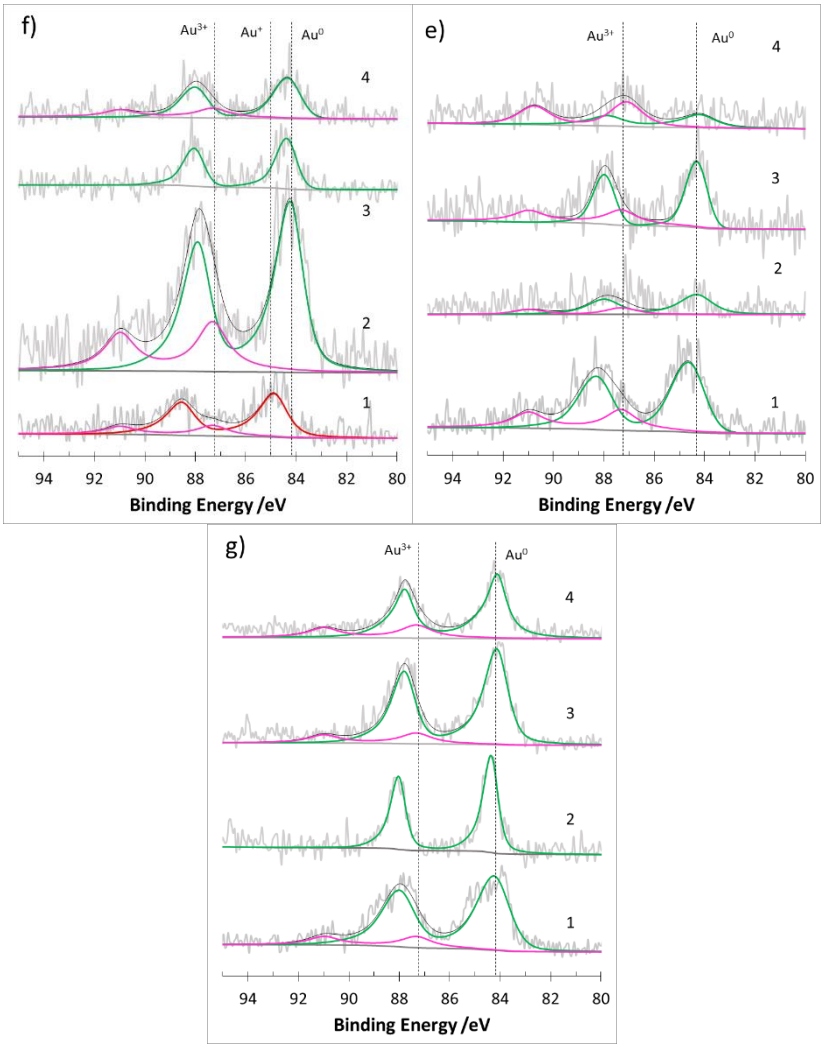

Figure 3.3: XPS of Au 4f region of 1% Au on a) 4.7 PZC Norit ROX HNO_3, b) 5.7 PZC Norit ROX AR, c) 3 PZC Timrex HNO_3, d) 3 PZC Timrex AR, e) 7.7 PZC Norit ROX, f) 4.2 PZC VXC-72, g) 3 PZC KBM where 1) unreduced, 2) unreduced pretreated, 3) reduced, 4) reduced pretreated

A 0.8% Au catalyst supported on unoxidized Norit ROX was also synthesized and analyzed with XPS and XRD. The XRD shown in Figure 3.2e displays a similar trend to the samples made on AR oxidized Norit ROX where there is no visible Au[111] peak after synthesis or pretreatment. The only gold seen is after reduction but upon pretreatment the particles redisperse. The Au 4f region of this catalyst shown in Figure 3.3e only shows Au(III) and Au(I) after synthesis which is unique to this sample. When reduced only

metallic Au is seen. After pretreatment of both the unreduced and reduced samples there is an increase in the relative intensity of Au(III). The Cl 2p region of the XPS shows that Au(III) in the form of $AuCl_3$ is present in all samples. Even without oxidation Norit ROX has the ability to stabilize atomically dispersed Au.

XRD was also done on catalysts made with Darco-KBM and oxidized Vulcan XC-72. KBM is a high surface area carbon with a surface area of 1200 m^2/g and was used as a comparison to the high surface area Norit-ROX. The 0.9% Au on 3 PZC KBM in Figure 3.3g had unreduced and reduced particle sizes of 10 and 12 nm respectively. The unreduced pretreated and reduced pretreated samples grew to 14 and 17 nm. This is the typical trend. The large particle sizes suggest that even though there is a large surface there are not many stable binding sites for atomically dispersed Au. The 1.1% Au on 4.2 PZC HNO_3 oxi VXC shown in Figure 3.2f were more stable than on Timrex but not as stable as the Norit samples. The XRD of the unreduced catalyst show no significant Au peak suggesting atomic dispersion or particle sizes below the limit of detection. Upon pretreatment the unreduced sample shows a small Au[111] peak corresponding to a particle size on 10 nm. The reduced sample shows a broad peak corresponding to a particle size of 2.7 nm. The peak area of the reduced sample is much larger than that of the unreduced pretreated sample suggesting that there is some stability of the Au before reduction. The reduced pretreated sample shows particle growth to 8 nm without a significant change in peak area.

DFT studies have been done that show the most stable site for $AuCl_3$ species to be bound is on a carbonyl or a hydroxyl group.[33,34] The oxidized Norit with its large surface area has more carbonyl groups than most carbons making it an ideal support for atomic dispersion of Au. The lack of suitable binding sites on Timrex and other carbons allows for

the Au to be mobile in the presence of HCl and sinter. Additionally, Norit ROX ability to adsorb HCl onto its surface increases the stability of the catalyst by having more readily available Cl for the atomically dispersed to bind with during the reaction mechanism.

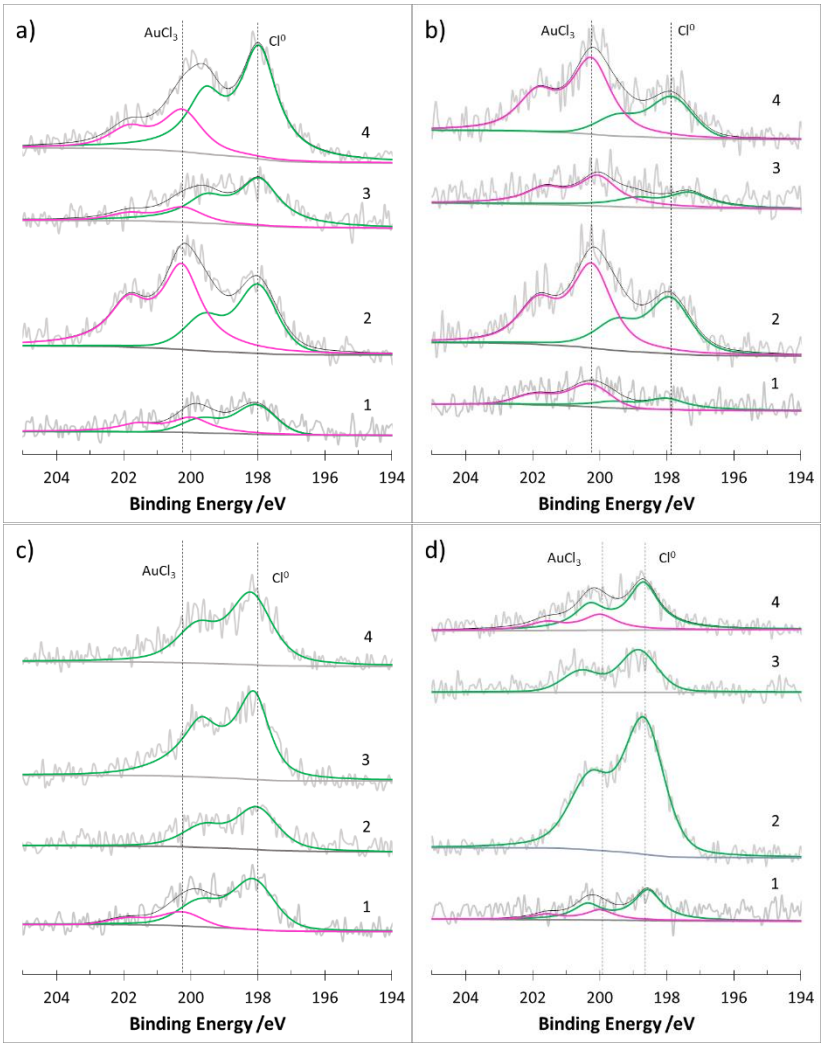

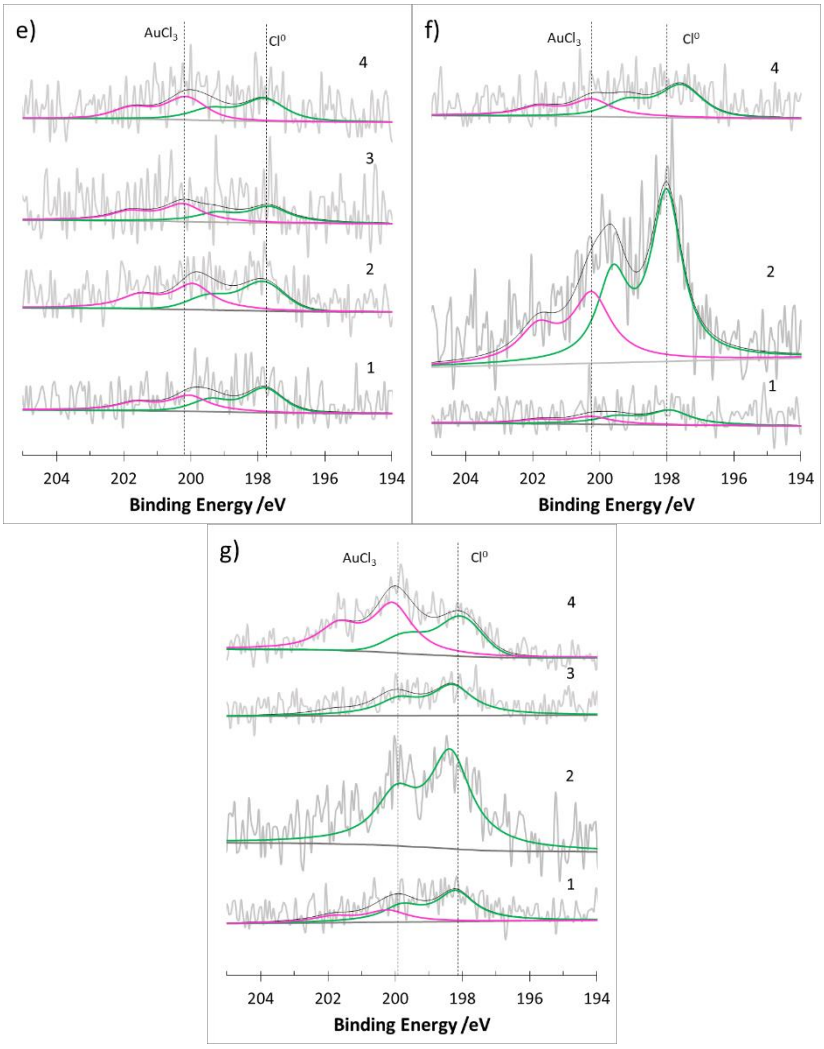

Figure 3.4: XPS of Cl 2p region of 1% Au on a) 4.7 PZC Norit ROX HNO3, b) 5.7 PZC Norit ROX AR, c) 3 PZC Timrex HNO3, d) 3 PZC Timrex AR, e) 7.7 PZC Norit ROX, f)4.2 PZC VXC-72 HNO3, g) 3 PZC KBM where 1) unreduced, 2) unreduced pretreated, 3) reduced, 4) reduced pretreated

3.4 Surface Defects and Chloride Saturation

XPS studies were done on the Norit ROX and Timrex supports to determine the ability of each support to adsorb HCl shown in table 3.3 and Figure 3.6. Pretreated Norit ROX oxidized in both HNO_3 and aqua regia after pretreatment had a mass concentration of Cl of at 3.7% and 2.9% respectively while the Timrex supports only had a concentration of 1.2% and 1.4%.

The Cl 2p regions of the pretreated support only samples were analyzed it was found that organically and inorganically bound chloride is present. Organic chloride is where Cl is bound to carbon directly and inorganic chloride is where Cl atoms are bound in a water-soluble form to impurities such as in NaCl, $CaCl_2$ or, more likely as HCl complexes on quaternary amines.[78,79] The C 1s region also verifies that much of the Cl binds directly to carbon. The C-O bond ratio decreases after pretreatment in every sample whether support only or after Au adsorption and is the only bond that decreases in every case. This leads us to believe that it is a binding site for Cl where HCl reduces the C-O resulting in the formation of a C-Cl bond and H_2O. This is chloride saturation, where chloride is adsorbed and directly bound to both the carbon surface and the atomically dispersed Au forming a stable and oxidized Au species. The Cl adsorption on the support may be able to be increased with increasing pretreatment time and temperature.

Table 3.3: Ratios of carbon bonds from XPS C 1s region of support only

C1s % ratio	C=C	C-C	C-O	O-C=O	Carbonates	π - π*
Norit ROX	57.8	13.7	8.8	5.0	5.7	9.1
Norit ROX HNO_3 oxi	54.1	13.8	9.2	6.8	6.2	10.0
Norit ROX HNO_3 oxi Pretreated	56.3	13.7	8.4	6.7	5.6	9.2
Norit ROX AR oxi	57.1	14.6	9.2	5.2	6.0	7.9
Norit ROX AR oxi pretreated	51.1	16.6	8.9	6.1	5.9	10.8
Timrex	61.8	12.0	8.2	4.4	4.5	9.2
Timrex HNO_3 oxi	63.0	12.1	8.7	4.7	4.6	7.1
Timrex HNO_3 oxi Pretreated	59.5	12.2	7.7	4.7	4.2	11.7
Timrex AR oxi	58.8	12.0	9.2	4.8	5.1	10.1
Timrex AR oxi pretreated	57.2	13.8	7.7	4.8	5.3	11.2

The C=C and the C-C peaks have sp^2 and sp^3 hybridization respectively, where sp^3 carbon hybridization is indicative of defects in the carbon matrix. It is obvious that Norit

ROX always has more defects (sp^3) than Timrex. This could be a possible explanation of the different properties of Norit. When normalized by mass of support it is clear to see that Norit has 5 times the amount of defect sites as shown in Figure 3.6. These defect sites near Cl bonded to the carbon support are ideal for stabilizing atomic Au and preventing sintering.

Norit ROX's ability to retain nearly three times the Cl than Timrex means that there is more Cl available to bind with the atomically dispersed Au for it to be catalytically active during the reaction process. The surface elemental analysis from the XPS yields some insightful information about each catalysts ability to adsorb Cl. In the case of the Au on AR oxidized Norit there is a significant increase in the mass of Cl on the surface after pretreatment from 0.6% to 2.5% in the unreduced with a similar trend seen in the reduced catalysts. This increase can be attributed to the increase in $AuCl_3$ as well as Cl bonded directly bonded to the surface of the support. The HCl disperses the Au and Cl is adsorbed onto the atomic Au. In contrast the Au on HNO_3 oxidized Timrex catalysts see a decrease in the surface concentration of Cl after pretreatment. The surface concentration of Cl mass concentration is reduced from 1.1% to 0.7% after pretreatment of the unoxidized catalyst. In this case the Au sinters rather than dispersing decreasing the available sites for Cl to be adsorbed.

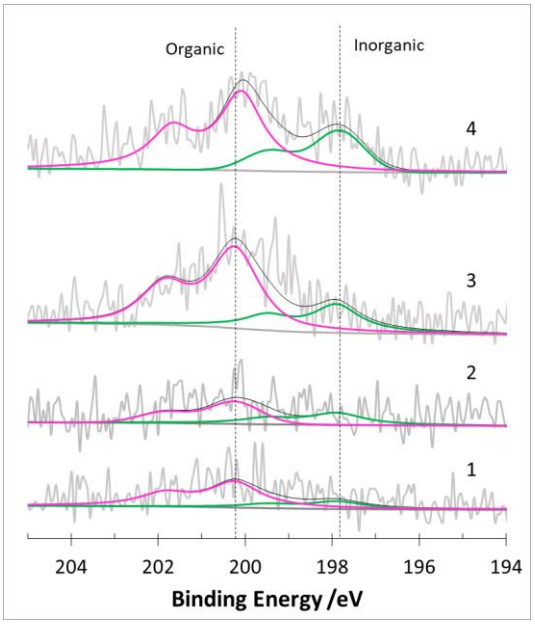

Figure 3.5: XPS of Cl 2p region of pretreated 1) AR oxidized Timrex, 2) HNO_3 oxidized Timrex, 3) AR oxidized Norit ROX, 4) HNO_3 oxidized Norit ROX

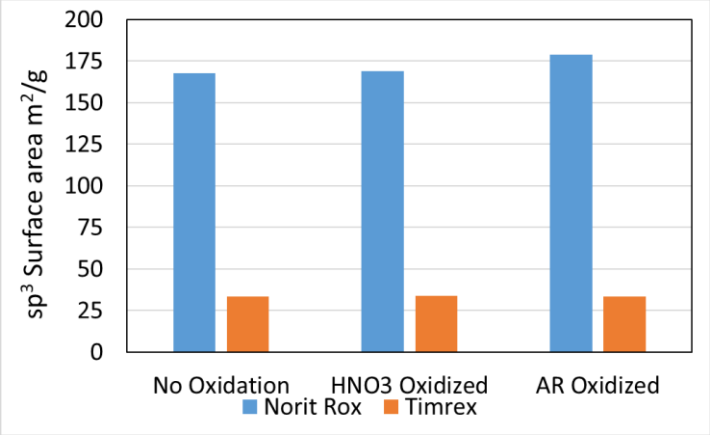

Figure 3.6: Surface area of defect sites

When comparing the mass concentration % of Cl as shown in Figure 3.7 it is clear to see that Norit is far superior to Timrex in retaining Cl with or without Au. In fact, Norit adsorbs more Cl when there is no gold present. All the catalysts have Cl present before pretreatment because Cl is in the $Au(en)_2Cl_3$ precursor used in SEA. All of the Au on Norit

catalysts begin with similar Cl content before pretreatment and have similar levels after pretreatment showing that the different oxidation processes did not affect Cl adsorption onto the catalysts as shown in Figure 3.7. The Timrex catalyst and support only samples all had about one third of the uptake of Cl compared to Norit. There is one discrepancy that comes from the unreduced pretreated 1.2% Au on AR oxidized Timrex. This sample had a large amount of Cl on the surface of 3.9%, which does not follow the expected trend. This is due to the formation of large NaCl particles forming on the surface. From XRD of this sample in Figure 3.3d there is a peak at 31.8 degrees that is attributed to NaCl and corresponds to 35 nm particles. This is verified by the XPS in Figure 3.5d where the peak attributed to Cl^0 at 198.6 eV is shifted to the left compared to the other Cl^0 peaks normally at 198.0 eV due to a large amount of NaCl. Washing the catalysts should result in a decrease in Cl content and result in a more accurate result from XPS.

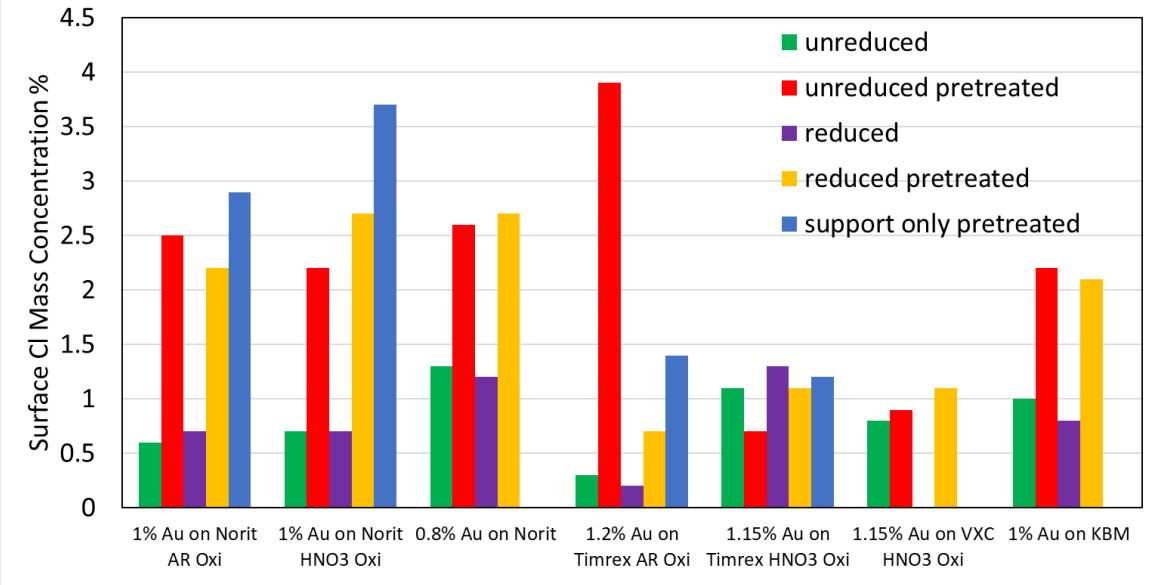

Figure 3.7: Surface concentration of Cl from XPS

3.5 Catalyst evaluation

Reaction data

The samples were evaluated in a vertical glass tube reactor at 180 °C for 24 hours after 30-minute pretreatment of 10 cc He and 11 cc HCl. After the pretreatment step 10 cc of C_2H_2 was introduced to the system already consisting of 21 cc of He and HCl. The reactor was loaded with 120 mg of catalysts and the resulting GSHV for Norit ROX, Timrex, and VXC-72 was 6200 $hr^{-1,}$ 4300 hr^{-1}, and 2300 hr^{-1} respectively which are several times larger than most literature. This was done to closely imitate industrial conditions and to keep the conversion low enough to see trends in reactivity. All catalysts reach a pseudo-steady state (characterized by the region in which the rate of deactivation is constant) within the first 1 – 10 hr.

Reactivity results are summarized for the three carbon supports and pretreatments in Figure 3.8. From Figure 3.8b a trend is observed between Timrex, and acid used to oxidize on conversion. 1% Au on 3 PZC Timrex both oxidized by HNO_3 and Aqua Regia has the highest activity once pseudo-steady state is reached. Up until about 10 hours online Au on HNO_3 and Aqua Regia oxidized Timrex of similar PZC behaved the same. After 10 hours the Aqua Regia oxidized catalysts had a lower rate of decay and even seems to stabilize over time. However as seen in Figure S4 when the gold on Timrex catalysts are run for a longer time deactivation does occur.

There is not a significant difference between the different catalysts for the VXC-72 series in Figure 3.8c. For the VXC-72 series the 1% Au on the AR and HNO_3 oxidized support show similar conversion at every PZC. The only catalyst that performed differently was the 1% Au on the unoxidized VXC-72. This catalyst had a noticeably lower activity

possibly due to the lack of hydroxyl groups on the surface of the support. For the first 10 hours online the catalysts on HNO_3 oxidized VXC-72 have similar conversion and deactivation as the catalysts on AR oxidized VXC-72 with similar PZC. This leads us to believe that the acid used to oxidize has no effect on conversion for the VXC-72 series. The Au on the unoxidized VXC-72 support had an activity much lower than any of the other catalysts. This is similar to what others have reported.[68,80–83] The deactivation rate of each catalyst was similar after reaching pseudo steady-state after 10 hours online.

The Norit ROX series (Figure 3.8a) is clearly most active and stable catalyst. The most stable catalyst with the lowest deactivation rate is the 1% Au on 5.7 PZC HNO_3 oxidized Norit ROX. This catalyst has an acetylene conversion of 31% at 24 hours and 29% at 48 hours. This catalyst was run for 96 hours total and had a conversion of 23% resulting in an overall deactivation rate of 0.1%/hr. The 0.8% Au on untreated Norit ROX had a higher acetylene conversion of 40% at 24 hours and 28% at 48 hours, but a deactivation rate of 0.5%/hr. The lower initial conversion of the oxidized supports may be attributed to the pore structure being damaged during oxidation. The faster deactivation of Au on untreated Norit ROX catalyst is due to a lack of binding sites for the molecularly dispersed $AuCl_3$ species that can be gained from oxidation. The HNO_3 oxidized Norit catalysts were more stable and active than the AR oxidized catalyst despite the latter having more atomically dispersed Au after pretreatment. This may be due to the pore structure being damaged by the AR causing transport limitations and resulting in lower activity.

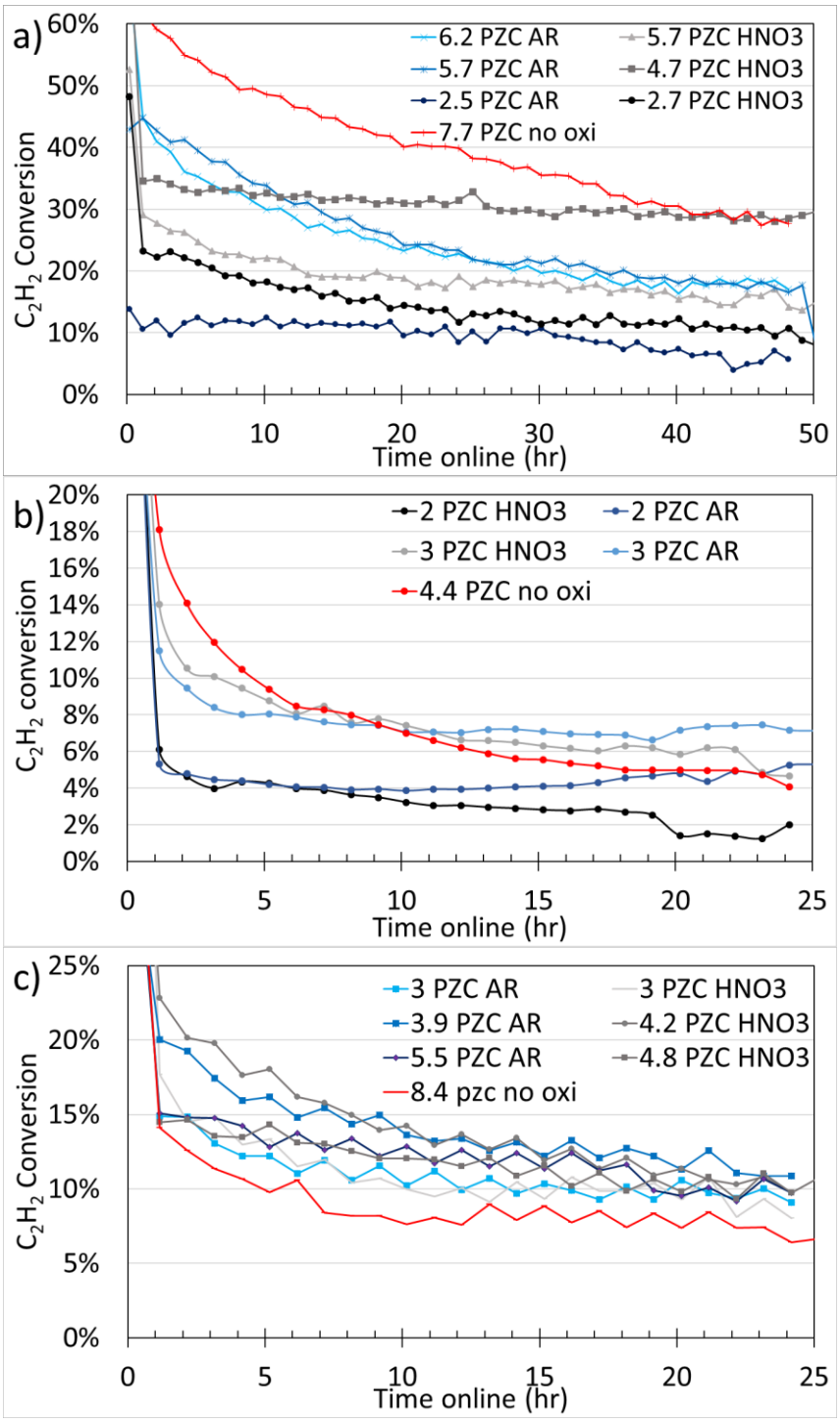

Figure 3.8: Catalytic performance of gold catalysts supported on oxidized a) Norit ROX b) Timrex, and c) VXC-72 as a function of reaction time.

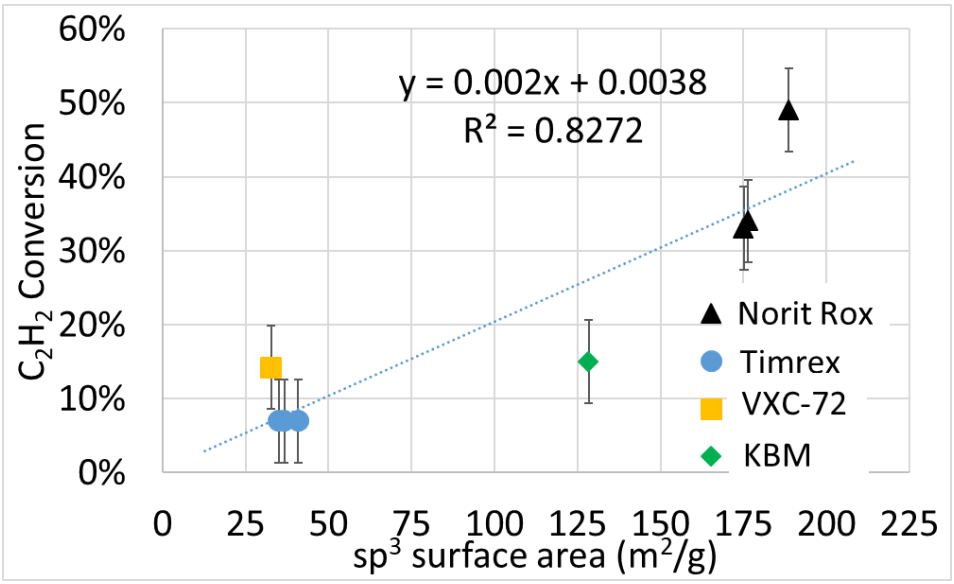

Figure 3.9: Comparison of acetylene conversion at 10 hours online and sp^3 surface area

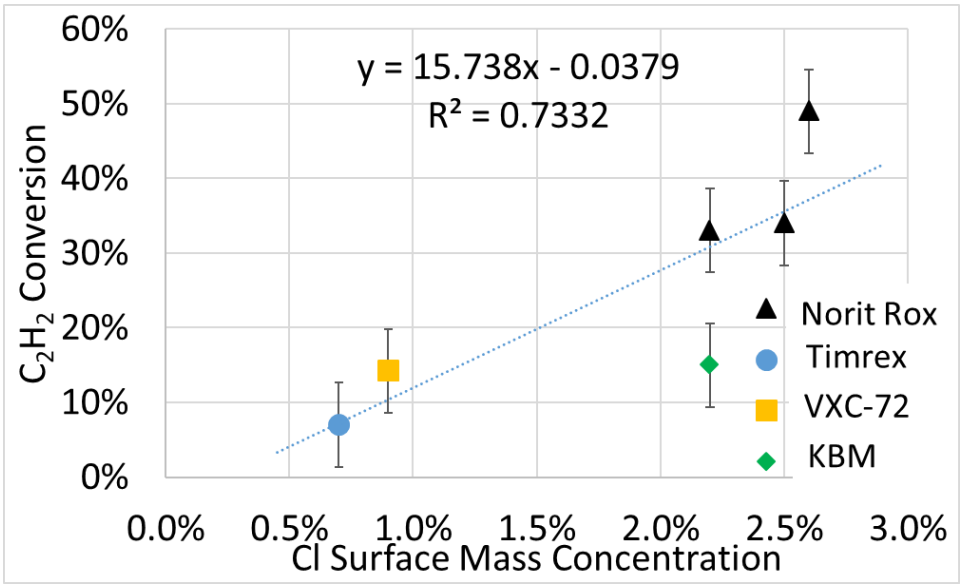

Figure 3.10: Comparison of acetylene conversion at 10 hours online and Cl uptake during pretreatment

Correlation of the reactivity data with the characterization data leads to two interesting connections. First, when acetylene conversion is compared to sp^3 surface area a clear trend arises. This is shown in Figure 3.9. The sp^3 surface area, indicative of defect site area, might provide stable binding sites for the $AuCl_3$ active site on the carbon surface,

so explaining the higher activity and stability of Norit ROX compared to the other carbons. Commensurately, as shown in Figure 3.10, there is a correlation between organic Cl retention after pretreatment and acetylene conversion at 10 hours. The amount of organic chloride retained is directly related to the number of active sites available after pretreatment. The 10-hour time online was chosen as at this time the deactivation rate for most catalysts has become constant.

Table 3.4: Catalyst Comparison to literature

Catalyst	Au wt %	gVCM/gAu hr @24 hr	gVCM/gCat hr @24hr
Au/Norit ROX 4.7 PZC HNO_3 oxi	1	432	4.3
Au/Norit ROX 5.7 PZC AR oxi	1	327	3.3
Au/Norit 7.7 PZC no oxi	0.8	696	3.9
Au/VXC Oxi [46]	1	281	2.8
$Au(CS(NH_2)_2)_2$ /Norit ROX [11]	0.1	1590	1.59
$HAuCl_4 + (NH_4)_2S_2O_3$/Norit ROX [84]	1	128	1.3
Au/Norit ROX – DMSO solvent	1	612	6.1
Au/Norit ROX – Acetone solvent	1	962	9.6

Table 3.4 shows some of the most active catalysts for acetylene hydrochlorination made by Graham Hutchings' groups compared to those made in the Regalbuto Group. The $Au(CS(NH_2)_2)_2$ /Norit ROX catalyst is from a study of Hutchings' where it was concluded that ligands containing soft donor atoms like cyanides and thiosulfate display greater stability in higher oxidation states over complexes that contain hard donor ligands.[11] The $HAuCl_4 + (NH_4)_2S_2O_3$/Norit ROX catalyst is from a patent with the same line of thinking in mind where they exchange the Cl ligands with thiosulfate ligands during synthesis.[84] These are arguably some of the best catalysts in literature but our catalysts made using SEA outperform them. The best overall catalysts are those made using an organic solvent rather

than water with a production rate of 9.6 and 6.1 gVCM/gCat hr from some of the newest work done by Hutchings. The catalysts made on oxidized Norit via SEA of $Au(en)_2Cl_3$ have comparable rates to the catalysts made using organic solvents with production rate of 4.3 and 3.9 gVCM/gCat hr.

3.6 Conclusion

In conclusion Norit ROX carbon as substrate for Au/C for the acetylene hydrochlorination reaction results in greater activity and stability when compared to other carbon support. The hydroxyl group content of the oxidized supports facilitates high uptake of the $Au(en)_2Cl_3$ during SEA. Additionally, oxidized Norit ROX has 5 times more defect sites when compared to oxidized Timrex. XPS studies revealed that Norit Rox has 5 times the surface area of sp^3 hybridized carbon, also known as defect sites in the predominant sp^2 hybridized carbon substrate, when compared to Timrex. These defects sites are stable binding sites for the active $AuCl_3$ site. During HCl pretreatment gold nanoparticles on most carbon supports sinter, but because Norit Rox has an abundance of stable binding sites for the active $AuCl_3$ species, the HCl pretreatment results in a redispersion of Au, including nanoparticles up to 4 nm in size, into atomically dispersed $AuCl_3$. Norit Rox also has the ability to adsorb up to 3 times more Cl onto its surface during pretreatment permitting the addition of Cl to Au during the reaction process. There is a direct correlation between the sp^3 surface area and the acetylene conversion and Cl adsorption during pretreatment and reaction. Catalysts made using SEA with a $Au(en)_2Cl_3$ precursor was able to make atomically dispersed Au on Norit ROX that was superior to the traditional $HAuCl_4$ and Aqua Regia method. These catalysts still deactivated slowly over time due to sintering. When compared to the leading catalysts made with the traditional $HAuCl_4$ and aqua regia

method, catalysts synthesized by SEA using $Au(en)_2Cl_3$ precursor are more active and stable.

Chapter 4

Conclusion: Future Work

4.1 Norit surface study

The understanding that Norit ROX is the ideal carbon support compared to others due to its abundance of hydroxyl groups, sp^3 hybridized C-C bonds that are defects on the carbon surface and its superior ability to adsorb Cl leads us to believe that further modification can be done to the support to further optimize it. Additionally, during the study the catalysts were exposed to acetone in the feed stream, which is known to inhibit the reaction, from the acetylene source. If this acetone is removed from the stream with a filter the catalyst should be even more active and stable.

There has been success in decreasing the gold loading on Norit ROX support and making a stable catalyst down to 0.1 wt%.[12] A lower amount of Au may reduce the ability of the atomically dispersed gold from agglomerating before attaching to a Cl and being anchored once again to the surface. Therefore, an investigation into decreasing or increasing the gold loading on the oxidized Norit ROX support needs to be done. An excess of HCl is known to be increase the conversion of the acetylene hydrochlorination reaction over gold due to the rate limiting step being the adsorption of HCl onto the Au site but with the evidence that HCl has the ability to redisperse small Au nanoparticles on oxidized Norit ROX the exact ratio needs to be optimized for these catalysts. Increasing the ratio of HCl

to acetylene to 1.5:1 or 2:1 in the reaction feed may result in higher activity and stability due to excess Cl binding to the surface and being able to combine with the atomically dispersed gold before agglomeration and pushing the equilibrium to the VCM product increasing the conversion.

Catalyst regeneration should be possible for this Au on Norit catalyst due to the evidence that nanoparticle sized Au can be dispersed under pretreatment conditions. Regeneration of the catalysts by washing with water to remove NaCl buildup followed by drying under a vacuum and finally being exposed to HCl at 180° C for an extended period should be enough to disperse Au from large nanoparticles back to the $AuCl_3$ species.

Nitrogen doped carbon has been used in several studies and has been shown to increase the activity and stability in the acetylene hydrochlorination.[85–88] However nitrogen doped oxidized Norit ROX has never been used as a support for SEA of $Au(en)_2Cl_3$ for acetylene hydrochlorination. Li et al showed in 2019 that gold on nitrogen doped Norit ROX has been shown to be highly resistant to sintering compared to tradition DI made catalysts and only deactivating due pore blockage and not sintering. Synthesizing a high weight loading of atomically dispersed gold via SEA onto a support that can strongly anchor the gold will have high conversion and stability.

References

(1) Haruta, M.; Kobayashi, T.; Sano, H.; Yamada, N. Novel Gold Catalysts for the Oxidation of Carbon Monoxide at a Temperature Far below 0 C. *Chem. Lett.* **1987**, 405–408.

(2) Hutchings, G. J. Vapor Phase Hydrochlorination of Acetylene: Correlation of Catalytic Activity of Supported Metal Chloride Catalysts. *J. Cata* **1985**, *96*, 292–295.

(3) Nkosi, B.; Coville, N. J.; Hutchings, G. J. Reactivation of a Supported Gold Catalyst for Acetylene Hydrochlorination. *J. Chem. Soc.* **1988**, 71–72.

(4) Andreeva, D.; Idakiev, V.; Tabakova, T.; Andreev, A.; Giovanoli, R. Low-Temperature Water-Gas Shift Reaction on Au / c -Fe203 Catalyst. *Appl. Catal.* **1996**, *134*, 275–283.

(5) Bond, G. C.; Sermon, P. A. Gold Catalysts for Olefin Hydrogenation Transmutation of Catalytic Properties. **1973**, No. 6, 102–105.

(6) Bond, G. The Early History of Catalysis by Gold. *Gold Bull.* **2008**, *41* (3), 235–241.

(7) Mcewan, L.; Julius, M.; Roberts, S.; Fletcher, J. C. Q. A Review of the Use of Gold Catalysts in Selective Hydrogenation Reactions. *Gold Bull.* **2010**, *43* (4), 298–306.

(8) Hutchings, G. J.; Grady, D. T. Hydrochlorination of Acetylene: The Effect of Mercuric Chloride Concentration on Catalyst LIfe. *Appl. Catal.* **1985**, *17*, 155–160.

(9) Hutchings, G. J. Catalysis: A Golden Future. *Gold Bull.* **1996**, *29* (4), 123–130.

(10) Liu, X.; Conte, M.; Elias, D.; Lu, L.; Morgan, D. J.; Freakley, S. J.; Johnston, P.; Kiely, J.; Hutchings, G. J. Investigation of the Active Species in the Carbon-Supported Gold Catalyst for Acetylene Hydrochlorination. *Catal. Sci. Technol.* **2016**, *6*, 5144–5153.

(11) Johnston, P.; Carthey, N.; Hutchings, G. J. Discovery, Development, and Commercialization of Gold Catalysts for Acetylene Hydrochlorination. *J. Am. Chem. Soc.* **2015**, *137*, 14548–14557.

(12) Kondrat, S. A.; Freakley, S. J.; Davies, C. J.; Lu, L.; Dawson, S.; Thetford, A.; Gibson, E. K.; Morgan, D. J.; Jones, W.; Wells, P. P.; et al. Identification of Single-Site Gold Catalysis in Acetylene Hydrochlorination. *Catalysis* **2017**, *1403* (March), 1399–1403.

(13) Lekhal, A.; Glasser, B. J.; Khinast, J. G. Impact of Drying on the Catalyst Profile in Supported Impregnation Catalysts. *Chem. Eng. Sci.* **2001**, *56* (15), 4473–4487.

(14) Conte, M.; Carley, A. F.; Hutchings, G. J. Reactivation of a Carbon-Supported Gold Catalyst for the Hydrochlorination of Acetylene. *Catal. Letters* **2008**, *124* (3–4), 165–167.

(15) Zhao, J.; Xu, J.; Xu, J.; Ni, J.; Zhang, T.; Xu, X.; Li, X. Activated-Carbon-Supported Gold-Cesium(I) as Highly Effective Catalysts for Hydrochlorination of Acetylene to Vinyl Chloride. *Chempluschem* **2015**, *80* (1), 196–201.

(16) Riahi, G.; Guillemot, D.; Polisset-Thfoin, M.; Khodadadi, a a; Fraissard, J. Preparation, Characterization and Catalytic Activity of Gold- Based Nanoparticles on HY Zeolites. *Catal. Today* **2002**, *72* (1–2), 115–121.

(17) Li, G.; Li, W.; Zhang, J. Strontium Promoted Activated Carbon-Supported Gold Catalysts for Non-Mercury Catalytic Acetylene Hydrochlorination. *Catal. Sci. Technol.* **2016**, *6* (9), 3230–3237.

(18) Zhou, K.; Wang, W.; Zhao, Z.; Luo, G.; Miller, J. T.; Wong, M. S.; Wei, F. Synergistic Gold-Bismuth Catalysis for Non-Mercury Hydrochlorination of Acetylene to Vinyl Chloride Monomer. *ACS Catal.* **2014**, *4* (9), 3112–3116.

(19) Zhao, J.; Yu, Y.; Xu, X.; Di, S.; Wang, B.; Xu, H.; Ni, J.; Guo, L. L.; Pan, Z.; Li, X. Stabilizing Au(III) in Supported-Ionic-Liquid-Phase (SILP) Catalyst Using CuCl2 via a Redox Mechanism. *Appl. Catal. B Environ.* **2017**, *206*, 175–183.

(20) Zhao, J.; Gu, S.; Xu, X.; Zhang, T.; Yu, Y.; Di, X.; Ni, J.; Pan, Z.; Li, X. Supported Ionic-Liquid-Phase-Stabilized Au(III) Catalyst for Acetylene Hydrochlorination. *Catal. Sci. Technol.* **2016**, *6* (9), 3263–3270.

(21) Qi, X.; Chen, W.; Zhang, J. Highly Effective Carbon-Supported Gold-Ionic Liquid Catalyst for Acetylene Hydrochlorination. *RSC Adv.* **2019**, *9* (38), 21931–21938.

(22) Regalbuto, J. R. A Scientific Method to Prepare Supported Metal Catalysts. **2006**.

(23) Diao, W.; Tengco, J. M. M.; Regalbuto, J. R.; Monnier, J. R. Preparation and Characterization of Pt − Ru Bimetallic Catalysts Synthesized by Electroless Deposition Methods. *ACS Catal.* **2015**, *5*, 5123−5134.

(24) Regalbuto, J. R. Strong Electrostatic Adsorption of Metals onto Catalyst Supports. In *Catalyst preparation*; 2007; pp 297–318.

(25) Tengco, J. M. M.; Alsadat, B.; Mehrabadi, T.; Zhang, Y.; Wongkaew, A.; Regalbuto, J. R.; Weidner, J. W.; Monnier, J. R. Synthesis and Electrochemical Evaluation of Carbon Supported Pt-Co Bimetallic Catalysts Prepared by Electroless Deposition and Modified Charge Enhanced Dry Impregnation. *Catalysts* **2016**, *8* (83).

(26) Brunelle, J. P. Preparation of Catalysts by Adsorption of Metal Complexes on Mineral Oxides. *Stud. Surf. Sci. Catal.* **1979**, *3* (C), 211–232.

(27) Sverjensky, D. A.; Sahai, N. Theoretical Prediction of Single-Site Surface-Protonation Equilibrium Constants for Oxides and Silicates in Water. *Geochim. Cosmochim. Acta* **1996**, *60* (20), 3773–3797.

(28) Sverjensky, D. A. Interpretation and Prediction of Triple-Layer Model Capacitances and the Structure of the Oxide-Electrolyte-Water Interface. *Geochim. Cosmochim. Acta* **2001**, *65* (21), 3643–3655.

(29) Sverjensky, D. A.; Sahai, N. Theoretical Prediction of Single-Site Enthalpies of Surface Protonation for Oxides and Silicates in Water. *Geochim. Cosmochim. Acta* **1998**, *62* (23–24), 3703–3716.

(30) Sverjensky, D. A. Zero-Point-of-Charge Prediction from Crystal Chemistry and Solvation Theory. *Geochim. Cosmochim. Acta* **1994**, *58* (14), 3123–3129.

(31) Spieker, W. A.; Regalbuto, J. R. A Fundamental Model of Platinum Impregnation onto Alumina. *Chem. Eng. Sci.* **2001**, *56* (11), 3491–3504.

(32) Mehrabadi, B. A. T.; Eskandari, S.; Khan, U.; White, R. D.; Regalbuto, J. R. A Review of Preparation Methods for Supported Metal Catalysts. In *Advances in Catalysis*; 2017; Vol. 61, pp 1–35.

(33) Kaiser, S. K.; Lin, R.; Mitchell, S.; Fako, E.; Krumeich, F.; Hauert, R.; Safonova, O. V.; Kondratenko, V. A.; Kondratenko, E. V.; Collins, S. M.; et al. Controlling the Speciation and Reactivity of Carbon-Supported Gold Nanostructures for Catalysed Acetylene Hydrochlorination. *Chem. Sci.* **2019**, *10* (2), 359–369.

(34) Zhao, C.; Guan, Q.; Li, W. DFT Studies on the Mechanism of Acetylene Hydrochlorination over Gold-Based Catalysts and Guidance for Catalyst Construction. *Inorg. Chem. Front.* **2019**, *6* (10), 2944–2952.

(35) Kobayashi, T.; Haruta, M.; Sano, H.; Nakane, M. A Selective CO Sensor Using Ti-Doped α-Fe2O3with Coprecipitated Ultrafine Particles of Gold. *Sensors and Actuators* **1988**, *13* (4), 339–349.

(36) Sakurai, H.; Ueda, A.; Kobayashi, T.; Haruta, M. Low-Temperature Water–Gas Shift Reaction over Gold Deposited on TiO2. *Chem. Commun.* **1997**, No. 3, 271–272.

(37) Donoeva, B.; Masoud, N.; De Jongh, P. E. Carbon Support Surface Effects in the Gold-Catalyzed Oxidation of 5-Hydroxymethylfurfural. *ACS Catal.* **2017**, *7* (7), 4581–4591.

(38) Okumura, M.; Nakamura, S.; Tsubota, S.; Nakamura, T.; Azuma, M.; Masatake Haruta. Chemical Vapor Deposition of Gold on Al 2 O 3 , SiO 2 , and TiO 2 for the Oxidation of CO and of H 2. *Catal. Letters* **1998**, *51* (1–2), 53–58.

(39) Baatz, C.; Decker, N.; Prüße, U. New Innovative Gold Catalysts Prepared by an Improved Incipient Wetness Method. *J. Catal.* **2008**, *258* (1), 165–169.

(40) Dimitratos, N.; Lopez-Sanchez, J. A.; Morgan, D.; Carley, A.; Prati, L.; Hutchings, G. J. Solvent Free Liquid Phase Oxidation of Benzyl Alcohol Using Au Supported Catalysts Prepared Using a Sol Immobilization Technique. *Catal. Today* **2007**, *122* (3–4), 317–324.

(41) Sankar, M.; He, Q.; Morad, M.; Pritchard, J.; Freakley, S. J.; Edwards, J. K.; Taylor, S. H.; Morgan, D. J.; Carley, A. F.; Knight, D. W.; et al. Synthesis of Stable Ligand-Free Gold-Palladium Nanoparticles Using a Simple Excess Anion Method. *ACS Nano* **2012**, *6* (8), 6600–6613.

(42) Zanella, R.; Louis, C. Influence of the Conditions of Thermal Treatments and of Storage on the Size of the Gold Particles in Au / TiO 2 Samples. *Catal. Today* **2005**, *108*, 768–777.

(43) Block, B. P.; Bailar Jr., J. C. The Reaction of Gold (III) with Some Bidentate Coordinating Groups. **1948**, *432* (6), 4722–4723.

(44) Zhu, H.; Liang, C.; Yan, W.; Overbury, S. H.; Dai, S. Preparation of Highly Active Silica-Supported Au Catalysts for CO Oxidation by a Solution-Based Technique. *J. Phys. Chem. B* **2006**, *110*, 10842–10848.

(45) Minacheva, L. K.; Gladakya, A. S.; Sakharova, V. G.; Don, G. M.; Shchelkov, R. N.; Porai-Koshits, M. A. Crystalline and Molecular-Structure of AuenCl2bis (Ethyenediamine) Gold (III) Trichloride. *Russ. J. Inorg. Chem.* **1988**, *33*, 382–385.

(46) O'Connell, K. C.; Monnier, J. R.; Regalbuto, J. R. The Curious Relationship of Sintering to Activity in Supported Gold Catalysts for the Hydrochlorination of Acetylene. *Appl. Catal. B Environ.* **2018**, *225* (December 2017), 264–272.

(47) Raba, A. M.; Bautista-Ruíz, J.; Joya, M. R. Synthesis and Structural Properties of Niobium Pentoxide Powders: A Comparative Study of the Growth Process. *Mater. Res.* **2016**, *19* (6), 1381–1387.

(48) Zanella, R.; Giorgio, S.; Henry, C. R.; Louis, C.; Curie, M.; Cedex, P.; Cnrs, C.; Luminy, C. De. Alternative Methods for the Preparation of Gold Nanoparticles Supported on TiO 2. *J. Phys. Chem. B* **2002**, *106*, 7634–7642.

(49) Zanella, R.; Delannoy, L.; Louis, C. Mechanism of Deposition of Gold Precursors onto TiO2during the Preparation by Cation Adsorption and Deposition-Precipitation with NaOH and Urea. *Appl. Catal. A Gen.* **2005**, *291* (1–2), 62–72.

(50) Zanella, R.; Giorgio, S.; Shin, C.-H.; Henry, C. R.; Louis, C. Characterization and Reactivity in CO Oxidation of Gold Nanoparticles Supported on TiO2 Prepared by Deposition-Precipitation with NaOH and Urea. *J. Catal.* **2004**, *222* (2), 357–367.

(51) Aksu, S.; Doyle, F. M. Electrochemistry of Copper in Aqueous Ethylenediamine Solutions. *J. Electrochem. Soc.* **2002**, *149* (7), B340.

(52) Alshammari, A.; Kalevaru, V.; Martin, A. Bimetallic Catalysts Containing Gold and Palladium for Environmentally Important Reactions. *Catalysts* **2016**, *6* (7), 97.

(53) Makotchenko, E. V. Spectrophotometric Study of Complexation of Bis(Ethylenediamine)Gold(III) with the Chloride Ion in an Aqueous Solution. *Russ. J. Coord. Chem.* **2003**, *29* (10), 720–724.

(54) Gangopadhayay, A. K.; Chakravorty, A. Charge Transfer Spectra of Some Gold(III) Complexes. *J. Chem. Phys.* **1961**, *35* (6), 2206–2209.

(55) Mironov, I. V.; Afanas'eva, V. A. Gold(III) Amine Complexes in Aqueous Alkali Solutions. *Russ. J. Inorg. Chem.* **2010**, *55* (7), 1156–1161.

(56) McFarland, A. D.; Haynes, C. L.; Mirkin, C. A.; Van Duyne, R. P.; Godwin, H. A. Color My Nanoworld. *J. Chem. Educ.* **2004**, *81* (4), 544A.

(57) Cunningham, D.; Tsubota, S.; Kamijo, N.; Haruta, M. Preparation and Catalytic Behaviour of Sub-Nanometer Gold Deposited on TiO2 by Vacuum Calcination. *Res. Chem. Intermed.* **1993**, *19* (1), 1–13.

(58) Yuan, G.; Louis, C.; Delannoy, L.; Keane, M. A. Silica- and Titania-Supported Ni – Au : Application in Catalytic Hydrodechlorination. *J. Catal.* **2007**, *247*, 256–268.

(59) Sandoval, A.; Antonio, G.; Zanella, R.; Gabriela, D. Gold Nanoparticles : Support Effects for the WGS Reaction. *J. Mol. Catal. A Chem.* **2007**, *278*, 200–208.

(60) Zanella, R.; Sandoval, A.; Santiago, P.; Basiuk, V. A. New Preparation Method of Gold Nanoparticles on SiO 2. *J. Phys. Chem. B* **2006**, *110*, 8559–8565.

(61) Sakurai, H.; Akita, T.; Tsubota, S.; Kiuchi, M.; Haruta, M. Low-Temperature Activity of Au / CeO 2 for Water Gas Shift Reaction , and Characterization by ADF-STEM , Temperature-Programmed Reaction , and Pulse Reaction. *Appl. Catal. A Gen.* **2005**, *291*, 179–187.

(62) Besson, M.; Kallel, A.; Gallezot, P.; Zanella, R.; Louis, C. Gold Catalysts Supported on Titanium Oxide for Catalytic Wet Air Oxidation of Succinic Acid. *Catal. Commun.* **2003**, *4*, 471–476.

(63) Prati, L.; Rossi, M. Gold on Carbon as a New Catalyst for Selective Liquid Phase Oxidation of Diols. *J. Catal.* **1998**, *176*, 552–560.

(64) Okumura, M.; Tsubota, S.; Haruta, M. Preparation of Supported Gold Catalysts by Gas-Phase Grafting of Gold Acethylacetonate for Low-Temperature Oxidation of CO and of H2. *J. Mol. Catal. A Chem.* **2003**, *199* (1–2), 73–84.

(65) Ueda, A.; Oshima, T.; Haruta, M. Reduction of Nitrogen Monoxide with Propene in the Presence of Oxygen and Moisture over Gold Supported on Metal Oxides. *Appl. Catal. B Environ.* **1997**, *12*, 81–93.

(66) Lee, S.; Gavriilidis, A. Au Catalysts Supported on Anodised Aluminium for Low-Temperature CO Oxidation. *Catal. Commun.* **2002**, *3*, 425–428.

(67) Boyd, D.; Golunski, S.; Hearne, G. R.; Magadzu, T. Reductive Routes to Stabilized Nanogold and Relation to Catalysis by Supported Gold. *Appl. Catal. A Gen.* **2005**, *292*, 76–81.

(68) Zhu, M.; Wang, Q.; Chen, K.; Wang, Y.; Huang, C.; Dai, H.; Yu, F.; Kang, L.; Dai, B. Development of a Heterogeneous Non-Mercury Catalyst for Acetylene Hydrochlorination. *ACS Catal.* **2015**, *5* (9), 5306–5316.

(69) Zhou, K.; Wang, W.; Zhao, Z.; Luo, G.; Miller, J. T.; Wong, M. S.; Wei, F. Synergistic Gold-Bismuth Catalysis for Non-Mercury Hydrochlorination of Acetylene to Vinyl Chloride Monomer. *ACS Catal.* **2014**, *4* (9), 3112–3116.

(70) Conte, M.; Davies, C. J.; Morgan, D. J.; Davies, T. E.; Elias, D. J.; Carley, A. F.; Johnston, P.; Hutchings, G. J. Aqua Regia Activated Au/C Catalysts for the Hydrochlorination of Acetylene. *J. Catal.* **2013**, *297*, 128–136.

(71) Conte, M.; Carley, A. F.; Heirene, C.; Willock, D. J.; Johnston, P.; Herzing, A. A.; Kiely, C. J.; Hutchings, G. J. Hydrochlorination of Acetylene Using a Supported Gold Catalyst: A Study of the Reaction Mechanism. *J. Catal.* **2007**, *250* (2), 231–239.

(72) Conte, M.; Davies, C. J.; Morgan, D. J.; Davies, T. E.; Carley, A. F.; Johnston, P.; Hutchings, G. J. Modifications of the Metal and Support during the Deactivation and Regeneration of Au/C Catalysts for the Hydrochlorination of Acetylene. *Catal. Sci. Technol.* **2013**, *3* (1), 128–134.

(73) Conte, M.; Davies, C. J.; Morgan, D. J.; Davies, T. E.; Elias, D. J.; Carley, A. F.; Johnston, P.; Hutchings, G. J. Aqua Regia Activated Au/C Catalysts for the Hydrochlorination of Acetylene. *J. Catal.* **2013**, *297*, 128–136.

(74) Kaiser, S. K.; Lin, R.; Mitchell, S.; Fako, E.; Krumeich, F.; Hauert, R.; Safonova, O. V.; Kondratenko, V. A.; Kondratenko, E. V.; Collins, S. M.; et al. Controlling the Speciation and Reactivity of Carbon-Supported Gold Nanostructures for Catalysed Acetylene Hydrochlorination. *Chem. Sci.* **2019**, *10* (2), 359–369.

(75) Lai, H.; Wang, B.; Yue, Y.; Sheng, G.; Wang, S.; Feng, F.; Zhang, Q.; Zhao, J.; Li, X. An Alternative Carbon Carrier in Green Preparation of Efficient Gold/Carbon Catalyst for Acetylene Hydrochlorination. *ChemCatChem* **2019**, *11* (14), 3318–3326.

(76) Hao, X.; Barnes, S.; Regalbuto, J. R. A Fundamental Study of Pt Impregnation of Carbon: Adsorption Equilibrium and Particle Synthesis. *J. Catal.* **2011**, *279* (1), 48–65.

(77) Hao, X.; Spieker, W. A.; Regalbuto, J. R. A Further Simplification of the Revised Physical Adsorption (RPA) Model. *J. Colloid Interface Sci.* **2003**, *267* (2), 259–264.

(78) Tsubouchi, N.; Saito, T.; Ohtaka, N.; Nakazato, Y.; Ohtsuka, Y. Chlorine Release during Fixed-Bed Gasification of Coal Chars with Carbon Dioxide. *Energy and Fuels* **2013**, *27* (9), 5076–5082.

(79) Tsubouchi, N.; Saito, T.; Ohtaka, N.; Ohtsuka, Y. Evolution of Hydrogen Chloride and Change in the Chlorine Functionality during Pyrolysis of Argonne Premium Coal Samples. *Energy and Fuels* **2013**, *27* (1), 87–96.

(80) Zhao, J.; Gu, S.; Xu, X.; Zhang, T.; Di, X.; Pan, Z.; Li, X. Promotional Effect of Copper(II) on an Activated Carbon Supported Low Content Bimetallic Gold–Cesium(I) Catalyst in Acetylene Hydrochlorination. *RSC Adv.* **2015**, *5* (123), 101427–101436.

(81) Song, Q.-L.; Wang, S.-J.; Shen, B.-X.; Zhao, J.-G. Palladium-Based Catalysts for the Hydrochlorination of Acetylene: Reasons for Deactivation and Its Regeneration. *Pet. Sci. Technol.* **2010**, *28* (18), 1825–1833.

(82) Huang, C.; Zhu, M.; Kang, L.; Li, X.; Dai, B. Active Carbon Supported TiO2-AuCl3/AC Catalyst with Excellent Stability for Acetylene Hydrochlorination Reaction. *Chem. Eng. J.* **2014**, *242*, 69–75.

(83) Zhao, J.; Zeng, J.; Cheng, X.; Wang, L.; Yang, H.; Shen, B. An Au–Cu Bimetal Catalyst for Acetylene Hydrochlorination with Renewable γ-Al 2 O 3 as the Support. *RSC Adv.* **2015**, *5* (22), 16727–16734.

(84) Bishop, P.; Carthey, N. A. Wo 2013/008004 A2 (51), 2013.

(85) Wang, B.; Zhao, J.; Yue, Y.; Sheng, G.; Lai, H.; Rui, J. Carbon with Surface-Enriched Nitrogen and Sulfur Supported Au Catalysts for Acetylene Hydrochlorination. **2019**, *310014*, 1002–1009.

(86) Li, X.; Pan, X.; Bao, X. Nitrogen Doped Carbon Catalyzing Acetylene Conversion to Vinyl Chloride. *J. Energy Chem.* **2014**, *23* (2), 131–135.

(87) Zhao, J.; Zhang, T.; Di, X.; Xu, J.; Xu, J.; Feng, F.; Ni, J.; Li, X. Nitrogen-Modified Activated Carbon Supported Bimetallic Gold-Cesium(I) as Highly Active and Stable Catalyst for the Hydrochlorination of Acetylene. *RSC Adv.* **2015**, *5* (9), 6925–6931.

(88) Hu, J.; Yang, Q.; Yang, L.; Zhang, Z.; Su, B.; Bao, Z.; Ren, Q.; Xing, H.; Dai, S. Confining Noble Metal (Pd, Au, Pt) Nanoparticles in Surfactant Ionic Liquids: Active Non-Mercury Catalysts for Hydrochlorination of Acetylene. *ACS Catal.* **2015**, *5* (11), 6724–6731.

Appendix A

Additional Figures and Tables

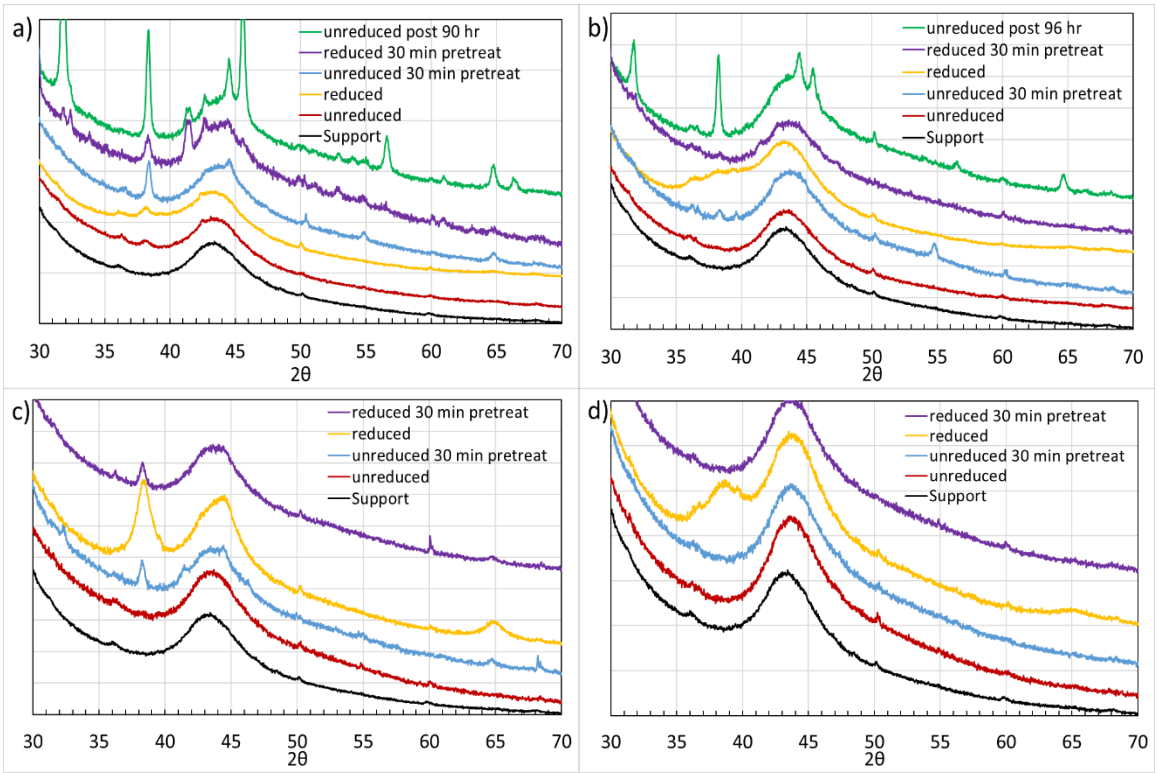

Figure A.1: XRD of a) 0.38% Au on 2.7 PZC HNO_3 oxidized Norit ROX b) 1.3% Au on 5.7 PZC HNO_3 oxidized Norit ROX, c) 1.1% Au on 2.5 PZC AR, d) 1% Au on 6.2 PZC AR oxidized Norit ROX

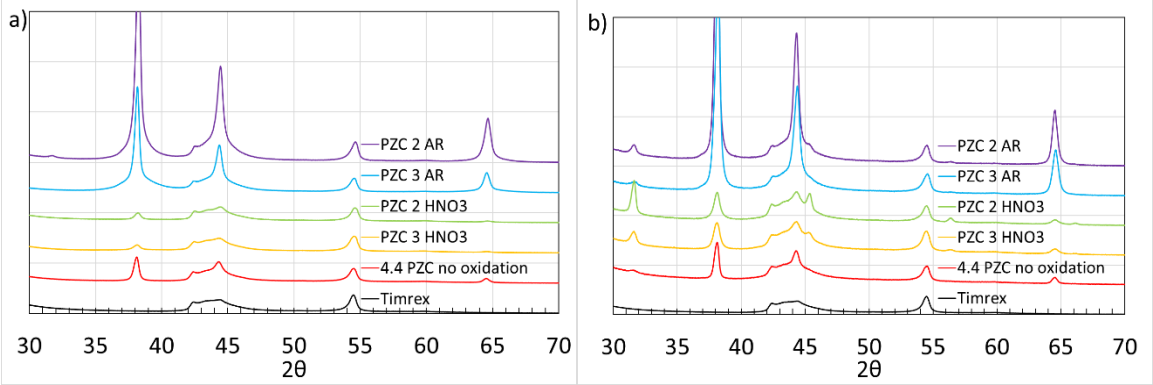

Figure A.2: XRD of reduced 1% Au on oxidized Timrex Series a) initial, b) post

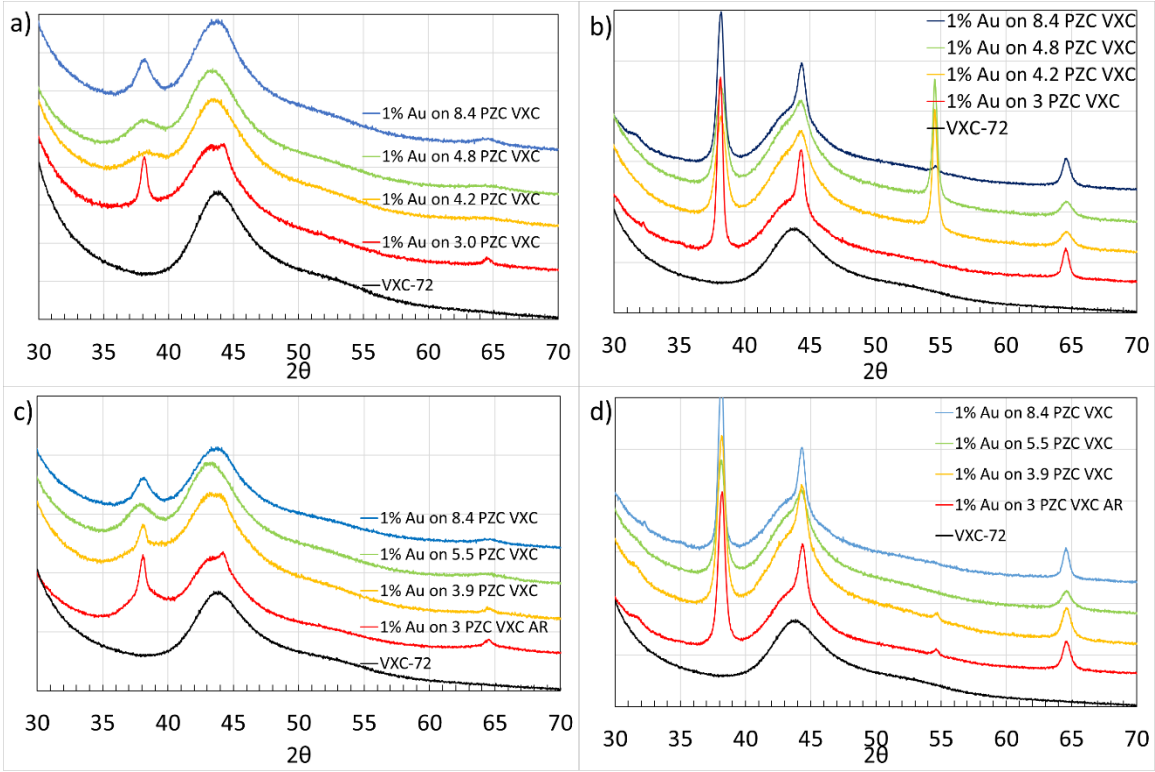

Figure A.3: XRD of 1% supported on a) HNO_3 oxidized VXC initial, b) HNO_3 oxidized VXC post, c) AR oxidized VXC initial, d) AR oxidized VXC post

Table A.1: Au particle sizes on various carbon supports before and after reaction

Support	Au wt%	Initial particle size (nm)	Reduced particle size (nm)	Post particle size (nm)
7.7 PZC Norit ROX		0	3.9	
5.7 PZC Norit ROX HNO_3 oxi	1.3	9.5	2.7	24.70
4.7 PZC Norit ROX HNO_3 oxi	1	11.4	3.5	25.4
2.7 PZC Norit ROX HNO_3 oxi	0.38	11.5	2.2	18.3
6.2 PZC Norit ROX AR oxi	1	0	3.7	
5.7 PZC Norit ROX AR oxi	1.1	0	3.6	
2.5 PZC Norit ROX AR oxi	1.1	0	6.1	
4.4 PZC Timrex	1	-	17.5	27.1
3 PZC Timrex HNO_3 oxi	1	-	11.1	21.9
2 PZC Timrex HNO_3 oxi	1	-	16.2	20.3
3 PZC Timrex AR oxi	1	-	12.3	22.3
2 PZC Timrex AR oxi	1	-	15.4	23.8
8 PZC VXC-72	1	-	5.5	16.1
4.8 PZC VXC-72 HNO_3 oxi	1	-	3.5	6.7
4.2 PZC VXC-72 HNO_3 oxi	1	-	3.1	10.7
3 PZC VXC-72 HNO_3 oxi	1	-	13.7	12.1
5.5 PZC VXC-72 AR oxi	1	-	2.8	10.4
3.9 PZC VXC-72 AR oxi	1	-	7.3	10.8
3 PZC VXC-72 AR oxi	1	-	6.7	12.8

Table A.2: Summary of peak rations from C 1s region of XPS of 1% Au on AR oxidized Norit ROX

C 1s	C=C	C-C	C-O	O-C=O	Carbonates	π - π^*
Norit unreduced	55.5	14.2	9.1	6.0	7.4	7.8
Norit unreduced pretreated	57.3	14.4	8.8	5.8	5.5	8.2
Norit reduced	56.5	14.3	9.4	5.6	5.5	8.7
Norit reduced pretreated	55.3	14.5	9.1	5.5	7.2	8.4

Table A.3:Summary of peak rations from O 1s region of XPS of 1% Au on AR oxidized Norit ROX

O 1s	C-O	C=O, OH
Norit unreduced	37.3	62.7
Norit unreduced pretreated	41.6	58.4
Norit reduced	40.8	59.2
Norit reduce pretreated	45.7	54.3

Table A.4: Summary of surface atomic concentrations on 1% Au on AR oxidized Norit ROX

Atomic Conc. %	Au	Cl	C	N	O	Na
Norit unreduced	0.1	0.2	91.5	2.3	5.2	0.7
Norit unreduced pretreated	0.1	0.9	91.8	1.3	5.2	0.7
Norit reduced	0.1	0.3	92.7	1.5	4.9	0.5
Norit reduce pretreated	0.1	0.8	92.5	1.7	4.4	0.5

Table A.5: Summary of surface mass concentrations on 1% Au on AR oxidized Norit ROX

Mass Conc. %	Au	Cl	C	N	O	Na
Norit unreduced	1.5	0.6	87.3	2.6	6.7	1.3
Norit unreduced pretreated	1.2	2.5	87.1	1.4	6.5	1.2
Norit reduced	2.2	0.7	88.2	1.7	6.3	0.9
Norit reduce pretreated	0.9	2.2	88.5	1.9	5.6	0.9

Table A.6: Summary of peak rations from C 1s region of XPS of 1% Au on HNO_3 oxidized Norit ROX

C 1s	C=C	C-C	C-O	O-C=O	Carbonates	π - π^*
Norit unreduced	55.9	14.2	9.8	6.2	5.2	8.6
Norit unreduced pretreated	56.8	14.3	9.4	5.8	5.3	8.5
Norit reduced	55.4	14.8	9.6	6.6	5.2	8.5
Norit reduced pretreated	55.5	15.7	8.9	6.4	5.3	8.3

Table A.7: Summary of peak rations from O 1s region of XPS of 1% Au on HNO_3 oxidized Norit ROX

O 1s	C-O	C=O, OH
Norit unreduced	27.9	72.1
Norit unreduced pretreated	41.7	58.3
Norit reduced	37.9	62.1
Norit reduce pretreated	66.9	33.1

Table A.8: Summary of surface mass concentrations on 1% Au on HNO_3 oxidized Norit ROX

Atomic Conc. %	Au	Cl	C	N	O	Na
Norit unreduced	0.3	0.3	90.6	2.0	6.4	0.8
Norit unreduced pretreated	0.1	0.8	92.0	1.5	5.3	0.3
Norit reduced	0.2	0.2	90.2	1.5	7.4	0.5
Norit reduce pretreated	0.1	1.0	90.6	2.0	5.8	0.5

Table A.9: Summary of surface mass concentrations on 1% Au on AR oxidized Norit ROX

Mass Conc. %	Au	Cl	C	N	O	Na
Norit unreduced	3.8	0.7	84.6	2.2	7.9	0.8
Norit unreduced pretreated	1.3	2.2	87.6	1.6	6.7	0.6
Norit reduced	2.6	0.7	84.9	1.7	9.3	0.8
Norit reduce pretreated	0.9	2.7	85.9	2.2	7.3	1.0

Table A.10: Summary of peak rations from C 1s region of XPS of 1.2% Au on AR oxidized Timrex

C 1s	C=C	C-C	C-O	O-C=O	Carbonates	π - π^*
Timrex unreduced	59.8	13.5	9.2	4.3	4.0	9.1
Timrex unreduced pretreated	60.3	13.1	8.0	4.3	3.9	10.3
Timrex reduced	61.3	13.8	8.8	4.2	4.2	7.6
Timrex reduce pretreated	63.1	12.9	7.8	4.1	4.0	8.2

Table A.11: Summary of peak rations from O 1s region of XPS of 1% Au on AR oxidized Timrex

O 1s	C-O	C=O, OH
Timrex unreduced	20.4	79.6
Timrex unreduced pretreated	40.5	59.5
Timrex reduced	29.4	70.6
Timrex reduce pretreated	37.6	62.4

Table A.12: Summary of surface atomic concentrations on 1.2% Au on AR oxidized Timrex

Atomic Conc. %	Au	Cl	C	N	O	Na
Timrex unreduced	0.1	0.1	94.0	1.5	3.9	0.4
Timrex unreduced pretreated	0.1	1.4	92.4	1.2	4.7	0.2
Timrex reduced	0.2	0.5	95.3	1.1	3.1	0.2
Timrex reduce pretreated	0.1	0.2	95.4	1.3	2.7	0.3

Table A.13: Summary of surface mass concentrations on 1.2% Au on AR oxidized Timrex

Mass Conc. %	Au	Cl	C	N	O	Na
Timrex unreduced	1.6	0.3	90.7	1.7	5.0	0.7
Timrex unreduced pretreated	0.7	3.9	87.7	1.3	6.0	0.4
Timrex reduced	0.7	0.2	93.2	1.2	4.0	0.4
Timrex reduce pretreated	1.4	0.7	92.4	1.5	3.5	0.5

Table A.14: Summary of peak rations from C 1s region of XPS of 1.2% Au on HNO_3 oxidized Timrex

C 1s	C=C	C-C	C-O	O-C=O	Carbonates	π - π^*
Timrex unreduced	61.2	12.4	8.3	4.8	4.3	9
Timrex unreduced pretreated	61.4	12.5	8.1	4.6	4.2	9.2
Timrex reduced	61.3	12.5	7.9	4.8	4.3	9.2
Timrex reduce pretreated	62.1	11.8	7.7	4.4	4.1	9.9

Table A.15: Summary of peak rations from O 1s region of XPS of 1.2% Au on HNO_3 oxidized Timrex

O 1s	C-O	C=O, OH
Timrex unreduced	36.8	63.2
Timrex unreduced pretreated	39.9	60.1
Timrex reduced	40.7	59.3
Timrex reduce pretreated	57.6	42.4

Table A.16: Summary of surface atomic concentrations on 1.2% Au on HNO_3 oxidized Timrex

Atomic Conc. %	Au	Cl	C	N	O	Na
Timrex unreduced	0.1	0.4	93.4	1.2	4.2	0.7
Timrex unreduced pretreated	0.1	0.3	93.7	1.2	3.2	1.5
Timrex reduced	0.1	0.5	94.1	0.7	3.9	0.7
Timrex reduce pretreated	0.1	0.4	94.1	1.3	3.4	0.7

Table A.17: Summary of surface mass concentrations on 1.2% Au on HNO_3 oxidized Timrex

Mass Conc. %	Au	Cl	C	N	O	Na
Timrex unreduced	1.3	1.1	89.5	1.4	5.3	1.4
Timrex unreduced pretreated	1.1	0.7	90.1	1.3	4.1	2.7
Timrex reduced	1.2	1.3	90.3	0.8	5.0	1.4
Timrex reduce pretreated	1.0	1.1	90.8	1.5	4.3	1.3

Table A.18: Summary of peak rations from C 1s region of XPS of 10.8 Au on 7.7 PZC Norit ROX

C 1s	C=C	C-C	C-O	O-C=O	Carbonates	π - π^*
Norit unreduced	57.2	14.1	9.4	5.1	5.2	8.9
Norit unreduced pretreated	49.8	15.4	10.9	5.6	9.0	9.2
Norit reduced	54.9	13.9	9.4	6.7	6.3	8.8
Norit reduced pretreated	53.8	14.1	10.4	5.9	6.4	9.5

Table A.19: Summary of peak rations from O 1s region of XPS of 0.8% Au on 7.7 PZC Norit ROX

O 1s	C-O	C=O, OH
Norit unreduced	49.4	50.6
Norit unreduced pretreated	52.7	47.3
Norit reduced	63.0	37.0
Norit reduce pretreated	55.1	44.9

Table A.20: Summary of surface atomic concentrations on 0.8% Au on 7.7 PZC Norit ROX

Atomic Conc. %	Au	Cl	C	N	O	Na
Norit unreduced	0.3	0.5	91.2	3.9	3.4	0.7
Norit unreduced pretreated	0.1	0.9	90.1	4.7	4.2	0.1
Norit reduced	0.2	0.4	89.5	3.3	5.8	0.8
Norit reduce pretreated	0.1	1.0	95.0	0	3.9	0

Table A.21: Summary of surface mass concentrations on 0.8% Au on 7.7 PZC Norit ROX

Mass Conc. %	Au	Cl	C	N	O	Na
Norit unreduced	4.3	1.3	84.6	4.2	4.3	1.3
Norit unreduced pretreated	2.1	2.6	84.9	5.1	5.3	2.1
Norit reduced	3.1	1.2	83.5	3.5	7.2	1.5
Norit reduce pretreated	2.3	2.7	90.0	0	5.0	0

Table A.22: Summary of surface atomic concentrations on Norit ROX

Atomic Conc. %	C	O	Cl
Norit ROX	94.8	5.2	0
Norit ROX HNO_3 oxidized	94.2	5.8	0
Norit ROX HNO_3 oxidized Pretreated	93.5	5.2	1.3
Norit ROX AR oxidized	93.1	6.9	0
Norit ROX AR oxidized pretreated	92.4	6.6	1.0

Table A.23: Summary of surface mass concentrations on Norit ROX

Mass Conc. %	C	O	Cl
Norit ROX	93.2	6.8	0
Norit ROX HNO_3 oxidized	92.4	7.6	0
Norit ROX HNO_3 oxidized Pretreated	89.7	6.6	3.7
Norit ROX AR oxidized	91.1	8.9	0
Norit ROX AR oxidized pretreated	88.7	8.4	2.9

Table A.24: Summary of surface atomic concentrations on Timrex

Atomic Conc. %	C	O	Cl
Timrex	96.5	3.5	0
Timrex HNO_3 oxidized	95.5	4.5	0
Timrex HNO_3 oxidized Pretreated	95.8	3.8	0.4
Timrex AR oxidized	95.2	4.8	0
Timrex AR oxidized pretreated	95.6	3.9	0.5

Table A.25: Summary of surface mass concentrations on Timrex

Mass Conc. %	C	O	Cl
Timrex	95.4	4.6	0
Timrex HNO_3 oxidized	94.2	5.8	0
Timrex HNO_3 oxidized Pretreated	93.8	5.0	1.2
Timrex AR oxidized	93.7	6.3	0
Timrex AR oxidized pretreated	93.5	5.1	1.4

Table A.26: Summary of peak rations from C 1s region of XPS of 1.15% Au on HNO_3 oxidized VXC-72

C 1s	C=C	C-C	C-O	O-C=O	Carbonates	π - π^*
VXC support only	59.3	13.0	6.8	4.8	6.0	10.1
VXC HNO_3 support only	58.0	12.4	7.7	4.7	6.5	10.6
VXC unreduced	58.9	11.0	8.1	5.0	7.6	9.4
VXC unreduced pretreated	60.3	12.9	8.0	4.6	4.9	9.4
VXC reduced	58.5	11.1	7.3	7.2	6.8	9.1
VXC reduce pretreated	56.8	11.0	8.1	6.8	6.5	10.7

Table A.27: Summary of peak rations from O 1s region of XPS of 1.15% Au on HNO_3 oxidized VXC-72

O 1s	C-O	C=O, OH
VXC support only	55.3	44.7
VXC HNO_3 support only	38.1	61.9
VXC unreduced	40.7	59.3
VXC unreduced pretreated	29.9	48.8
VXC reduced	47.9	70.1
VXC reduce pretreated	46.5	53.5

Table A.28: Summary of surface atomic concentrations on 1.15% Au on HNO_3 oxidized VXC-72

Atomic Conc. %	Au	Cl	C	N	O	Na
VXC support only	0	0	98.2	0	1.8	0
VXC HNO_3 support only	0	0	97.6	0	2.4	0
VXC unreduced	0.1	0.3	97.1	0	1.7	0.8
VXC unreduced pretreated	0.1	0.3	97.8	0.6	1.1	0.1
VXC reduced	0.1	0	97.4	0	1.7	0.8
VXC reduce pretreated	0.1	0.4	96.7	0	2.2	0.6

Table A.29: Summary of surface mass concentrations on 1.15% Au on HNO_3 oxidized VXC-72

Mass Conc. %	Au	Cl	C	N	O	Na
VXC support only	0	0	98.2	0	2.4	0
VXC HNO_3 support only	0	0	96.8	0	3.2	0
VXC unreduced	2.0	0.8	93.5	0	2.2	1.5
VXC unreduced pretreated	1.3	0.9	95.5	0.7	1.4	0.2
VXC reduced	2.1	0	94.1	0	2.2	1.6
VXC reduce pretreated	1.8	1.1	93.0	0	2.9	1.2

Table A.30: Summary of peak rations from C 1s region of XPS of 1% Au on 3 PZC KBM

C 1s	C=C	C-C	C-O	O-C=O	Carbonates	π - π^*
KBM support only	55.6	15.4	13.2	5.7	5	5.2
KBM unreduced	62.0	12.0	8.7	6.3	4.6	6.3
KBM unreduced pretreated	63.0	10.7	10.8	6.0	4.1	5.5
KBM reduced	63.5	11.4	8.8	5.6	4.1	6.6
KBM reduce pretreated	61.7	10.1	9.8	6.1	4.9	7.4

Table A.31: Summary of peak rations from O 1s region of XPS of 1% Au on 3 PZC KBM

O 1s	C-O	C=O, OH
KBM support only	20.2	79.8
KBM unreduced	27.6	72.4
KBM unreduced pretreated	28.2	71.8
KBM reduced	32.9	67.1
KBM reduce pretreated	45.9	54.1

Table A.32: Summary of surface atomic concentrations on 1% Au on 3 PZC KBM

Atomic Conc. %	Au	Cl	C	N	O	Na
KBM support only	0	0	9.06	0	12.1	0
KBM unreduced	0.2	0.4	89.5	0.9	8.7	0.3
KBM unreduced pretreated	0.2	0.8	88.6	1.2	8.6	0.6
KBM reduced	0.2	0.3	89.6	1.3	8.3	0.3
KBM reduce pretreated	0.2	0.8	89.7	8.9	0.4	0.2

Table A.33: Summary of surface mass concentrations on 1.15% Au on 1% Au on 3 PZC KBM

Mass Conc. %	Au	Cl	C	N	O	Na
KBM support only	0	0	87.9	0	12.1	0
KBM unreduced	2.9	1.0	83.8	1.0	10.8	0.5
KBM unreduced pretreated	2.5	2.2	82.2	1.3	10.7	1.1
KBM reduced	2.4	0.8	84.5	1.4	10.4	0.5
KBM reduce pretreated	2.3	2.1	83.8	11.0	0.8	2.3

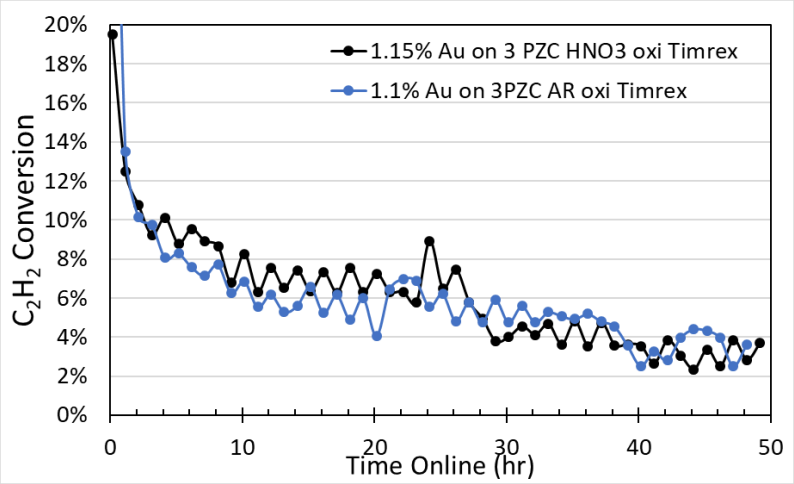

Figure A.4: Catalytic performance of unreduced Au supported on oxidized Timrex catalysts

Table A.34: Compilation of catalyst production rates

Support	Au wt %	gVCM/gAu hr @24 hr	gVCM/gCat hr @24 hr
Norit 7.7 PZC no oxi	0.8	696	5.6
Norit 2.7 PZC HNO_3 oxi	0.38	440	1.7
Norit 4.7 PZC HNO_3 oxi	1	432	4.3
Norit 5.7 PZC HNO_3 oxi	1.3	204	2.7
Norit 2.5 PZC AR oxi	1	118	1.2
Norit 4.7 PZC AR oxi	1	327	3.3
Norit 5.2 PZC AR oxi	1	318	3.2
VXC 8.4 PZC no oxi	1	89	1.1
VXC 3 PZC HNO3 oxi	1	113	1.1
VXC 4.2 PZC HNO3 oxi	1	135	1.4
VXC 4.8 PZC HNO3 oxi	1	135	1.4
VXC 3 PZC AR oxi	1	126	1.3
VXC 3.9 PZC AR oxi	1	152	1.5
VXC 5.5 PZC AR oxi	1	135	1.4
Timrex 4.4 PZC no oxi	1	56	0.56
Timrex 2 PZC HNO_3 oxi	1	28	0.28
Timrex 3 PZC HNO_3 oxi	1.2	85	0.98
Timrex 2 PZC AR oxi	1	70	0.7
Timrex 3 PZC AR oxi	1.1	76	0.84
Precursor complex[11]	Au wt %	gVCM/gAu hr @24 hr	gVCM/gCat hr @24hr

$Au(CS(NH_2)_2)_2$	0.1	1590	1.59
$Na_3(Au(S_2O_3)_2$	0.1	1440	1.44
$KAu(CN)_2$	0.1	1423	1.42
$(NH_4)_3Au(S_2O_3)_2$	0.1	1256	1.26
$KAu(SCN)_4$	0.1	1239	1.24
$Ca_3[Au(S_2O_3)_2]_2$	0.1	1239	1.24
$Au(NCNH_2)_2$	0.1	921	0.92
$HAuCl_4$ + Aqua regia	1	87	0.87
$HAu(C_3Cl_3N_3O_3)_3Cl$	1	87	0.87
$[Au(P(NCH_2CH_2OCH_2CH_2)_3)_2]NO_3$	1	55	0.55
$[(AuCl)_2$dppe]	1	23	0.23
$[Au(en)_2]Cl_3$	1	23	0.23
$HauCl_4$ + H2O	1	18	0.18
Hutchings patent [84]	Au wt %	gVCM/gAu hr @24 hr	gVCM/gCat hr @24hr
$HAuCl_4 + (NH_4)_2S_2O_3$	1	128	1.3
$HAuCl_4$ +AR	1	123	1.2
$HAuCl_4$	1	28	0.3
$HAuCl_4 + (Na)_2S_2O_3$	1	151	1.5
$HAuCl_4$ + trichloroisocyanuric acid in methonal	1	123	1.2
New Hutchings paper (unpublished)	Au wt %	gVCM/gAu hr @24 hr	gVCM/gCat hr @24hr
Au/C - DMSO	1	612	6.1
Au/C - DMF	1	350	3.5
Au/C - cyclohexanone	1	131	1.3
Au/C - Acetone	1	962	9.6
O'Connell's Catalysts[46]	Au wt %	gVCM/gAu hr @24 hr	gVCM/gCat hr @24 hr
Au/VXC	1	150	1.5
Au/VXC Oxi	1	281	2.8
Au/CA 1	1	160	1.6
Au/KBM	1	281	2.8
Au/KBB	1	251	2.5